Lukas Seewald, BSc

Structure-to-property relationships for thermal transport in molecular crystals

MASTER'S THESIS

to achieve the university degree of

Diplom-Ingenieur

Master's degree program: Advanced Materials Science

submitted to

Graz University of Technology

Supervisor

Ao.Univ.-Prof. Dipl.-Ing. Dr.techn. Egbert Zojer

Institute of Solid State Physics

Co-Supervisor

Dr. Natalia Bedoya-Martinez

Graz, March 2019

AFFIDAVIT

I declare that I have authored this thesis independently, that I have not used other than the declared sources/resources, and that I have explicitly indicated all material which has been quoted either literally or by content from the sources used. The text document uploaded to TUGRAZonline is identical to the present master's thesis.

Date	Signature
……	……

Abstract

The aim of this thesis is to obtain thermal conductivities for several molecular crystals and subsequently, to establish structure-to-property relationships. The thermal conductivity is studied by means of lattice dynamics simulations. The phonon properties are obtained within the harmonic approximation and enter the Boltzman transport equation. Scattering processes among phonons are modeled using a phonon lifetime model, proposed by Bjerg et al., which relies on the material's Grüneisen parameter. This approach yields the full thermal conductivity tensor and furthermore, the result is determined by the three quantities: phonon mode heat capacity, group velocity and phonon lifetime. This is an advantage because it allows to study the individual constituents and, thereby, to gain a deeper insight into the underlying physics. It was found, that for larger molecules, the component of the thermal conductivity perpendicular to the layers of the molecular crystal increases, leading to an increased anisotropy in thermal conductivity. Furthermore, the internal anharmonicity was found to decrease for larger molecules, due to the reduced number of interfaces between the densely packed layers.

The materials investigated in this work are naphthalene, anthracene and pentacene, fluorene, biphenyl and polyparaphenylene.

Table of Contents

1. Introduction

Whenever two systems of different temperature are connected to each other, the system is not at thermodynamic equilibrium any more. Consequently, a flux of heat will be established to restore the system back to thermodynamic equilibrium. The rate at which heat transport from the hot to the cold side occurs is related to the temperature difference and to some material's dependent property, the thermal conductivity. For small temperature gradients, this non-equilibrium process of heat transport can be described in a linearized way by Fourier's Law:

$$j = -\kappa \nabla T \qquad (1.1)$$

The established heat flux j is linear proportional to the temperature gradient ∇T. The proportionality factor κ is termed thermal conductivity and characterizes the material's ability to transport heat. In essence, the formula is very similar to Ohm's Law for electric currents or Fick's Law of diffusion. If we stress the phonon picture, a temperature gradient indeed causes a concentration gradient of phonons, phonon diffusion restores the system to equilibrium.

Why should one bother about thermal conductivity in the first place? One field where transport of heat is of main interest is thermoelectricity. This field has dragged attention from both academia and industry because of its potentially huge range of application. Providing electricity by consuming nothing but thermal energy, in best-case waste heat, could help to use less primary energy sources to reduce emission of greenhouse gasses. The efficiency of thermoelectricity in a material is expressed as the figure of merit $ZT = (\sigma\alpha^2/\kappa)T$, which combines the key material properties, electrical conductivity σ and the Seebeck coeffiecient α. Consequently, ongoing research is aiming for materials with best trade-off between high electric conductivity and low thermal conductivity at the same time. For example, in single crystals of SnSe a figure of merit of 2.6 at 923K was reported. This material shows very low thermal conductivity of 0.23 $Wm^{-1}K^{-1}$ at 973K.[1]

Other than thermoelectricity there are many applications that don't seem to deal with thermal transport in the first place, however, for example in microelectronics thermal management is of utmost importance for proper operation. In devices, heat is generated by joule and recombination heating. To ensure stable device operation and prevent thermal runaway, the occurring heat has to be carried away sufficiently. Due to increasing power density and speed of integrated circuits, the

importance of thermal management is raised, thus thermal conductivity is a main constraint for material selection during the design process of a device.[2]

In recent years organic semiconductors have seen various different applications like organic photovoltaics, OLED's for displays and lighting as well as various sensor applications to name a few. Due to advances in chemical synthesis and process engineering organic semiconductors combine a huge functional variety with production routs, able to produce devices of all sizes on many different, even flexible substrates at competitive costs.[3] Despite the importance, thermal transport properties have seen a lot less research interest than optical and electronic transport properties.[4,5]

In solid state, thermal energy can be carried by electrons and quantized vibrations, phonons. The carriers travel at their group velocity until they scatter, which limits their mean free path and subsequently, limits thermal transport. In molecular crystals, electrons are localized at molecules in contrast to delocalized electrons in metals. Due to the lack of free electrons, the contribution of electrons to thermal transport is negligible in molecular crystals, leaving thermal transport over to phonons. Assuming a perfect single crystal without any defects and in the absence of free electrons, the only limitation to phonon transport arises from scattering among phonons. This consideration implies the temperature dependence of thermal conductivity to be T^{-1} at elevated temperatures. With lowering temperature, the number of thermally occupied phonons decreases, hence phonon-phonon interactions are reduced leading to a peak in thermal conductivity. Further lowering temperature causes a rapid decrease in thermal conductivity which is attributed to the decreasing phonon heat capacity.[6] In general, organic semiconductors show very low thermal conductivities in the range of 0.1-0.7 $Wm^{-1}K^{-1}$, comparable to amorphous solids.[5] Exemplary values for some common organic semiconductors at room temperature are 0.185 $Wm^{-1}K^{-1}$ for P3HT[7], 0.62 $Wm^{-1}K^{-1}$ for pentacene[4], 0.24 $Wm^{-1}K^{-1}$ for TPD[4], 0.5 $Wm^{-1}K^{-1}$ for Alq3[4] and 0.59 $Wm^{-1}K^{-1}$ for Polyaniline (PANI)[8]. All thermal conductivity measurements were conducted on thin films. The lowest value of any organic semiconductor was found for PCBM, showing a thermal conductivity of 0.05-0.06 $Wm^{-1}K^{-1}$ at room temperature.[9] An exceptionally high thermal conductivity was observed for Polyethylene single crystals exceeding 100 $Wm^{-1}K^{-1}$.[10,11]

Molecular Crystals

In general, molecular crystals are the crystalline bulk phase of organic molecules. Those molecules have a carbon backbone and can contain nearly all atoms from the periodic table. In the context of

this work, the meaning of organic molecules is narrowed to aromatic hydrocarbons because of their interesting electronic properties. In contrast to saturated hydrocarbons that are built from sp^3 hybridized carbon atoms, aromatic hydrocarbons contain a conjugated π-electron system. The pi-electrons originate from sp^2 hybridization, in which three sp^2 hybrid-orbitals are formed from the 2s orbital and two 2p orbitals. The resulting hybrid-orbitals are coplanar in the plane of the contributing p-orbitals and equally separated at an angle of 120° relative to each other. The remaining third p-orbital is oriented, perpendicular to the hybrid orbitals. The hybrid orbitals pointing at each other form so called σ-bonds and build the molecular skeleton. Due to the overlap of remaining p-orbitals, so called π-bonds are formed, leading to a delocalized electron density above and below the plane of the molecule. The conjugated π-electron system gives rise to many characteristic physical properties of molecular crystals. Most important is its effect on intermolecular interactions. Spatial fluctuations of π-electrons create a fluctuating dipole moment, which can induce a dipole in neighboring molecules. This in turn causes attractive forces proportional to the polarizability of the molecule. For short distances, so called van der Waals interactions increase rapidly and therefore favor a highly dense packing. Furthermore, van der Waals forces are rather weak compared to the covalent bonds within the molecule which has the effect, that molecules in solid phase are kept preserved as such almost entirely. Hence those materials are termed molecular crystals.[12]

The presence of entire molecules as the basis of the unit cell has some important implications on the vibrational properties. One aspect is the usually much larger number of atoms in the unit cell, leading to much more eigenmodes. In return, this could potentially allow for more phonon scattering reducing the thermal conductivity after all. Another effect of molecules as crystallographic basis is the occurrence of external and internal modes.[13] External modes, also termed intermolecular modes are oscillations, in which molecules move relative to each other and the molecules are not or only slightly distorted. Internal modes describe eigenmodes within the molecules, thus they are also referred to as intramolecular modes. Due to the difference in interaction strength between covalent bonds within the molecule and dispersion interactions between the molecules, external modes are of lower frequency compared to internal modes, however the separation might not always be present in the phonon band structure. Yet another issue of molecular crystals is anisotropic thermal transport. In the first place Neumann's principle states, that physical properties must obey the symmetry operations of the crystal. Hardly any molecular crystals solidify in a cubic lattice. Therefore, thermal conductivity for those materials is expressed

as a tensor. This tensor must include symmetry operations of the constituting point group. In addition, a molecule's distinct shape compared to spherical atoms as crystal basis, should increase the anisotropy in thermal transport furthermore.

To cut a long story short, thermal conductivity is an important material's property, relevant for many different applications but at the same time, knowledge about thermal transport is rather basic, especially for molecular crystals. To address this lack of understanding, the main objective of this thesis is to develop structure-to-property relationships for thermal transport in molecular crystals. More precisely, thermal transport will be modeled for a set of molecules (see Figure 1) that are chosen to answer the following questions:

- How does the molecules torsional degree of freedom (DOF) affect thermal transport?
- How does the overall size of the molecule affect thermal transport?

To answer the first question, the materials naphthalene, fluorene and biphenyl were chosen. Naphthalene is built from two fused benzene rings, whereas fluorene and biphenyl incorporate two phenylene rings. In the case of fluorene, a methylene group is located at the ortho-positions of both rings, hence it is also referred to as 2,2'-Methylenebiphenyl. The phenylene rings of biphenyl are connected only by a single bond, representing the connection with the least resistance against torsion along the molecular axis. It is assumed, that the methylene group in fluorene increases this moment of resistance against torsion thus limiting the torsional DOF. If naphthalene is twisted along its molecular axis, the entire benzene rings are deformed which should result in the least torsional DOF. Considering the equation for undamped oscillation of a simple spring, $\omega = \sqrt{k/m}$ with the spring constant k and the mass m, it can be concluded that an increased spring constant leads to higher frequency. As a consequence, the torsional eigenmodes of naphthalene should have the highest frequencies, followed by fluorene's and biphenyl's. How this affects then thermal transport is not known yet.

The second research question sets the focus on the size of the constituting molecule which could have multiple effects. In the first place, larger molecules should show increased intermolecular coupling of the π-electron system. If the increased coupling makes up for the increased mass of larger molecules, higher maximum external frequencies were possible. In return, phonon dispersion and group velocities would increase. Another effect of larger molecules is the reduced number of interfaces between molecules. From naphthalene over anthracene to pentacene, fewer molecules

are required to fill a gap of given distance. Consequently, along the long molecular axis fewer interfaces appear for pentacene than there are for naphthalene. Polyparaphenylene will be an extreme situation, modelled as an infinite chain without interfaces along the chain direction. After all, interfaces should play an important role with respect to anisotropy in thermal transport.

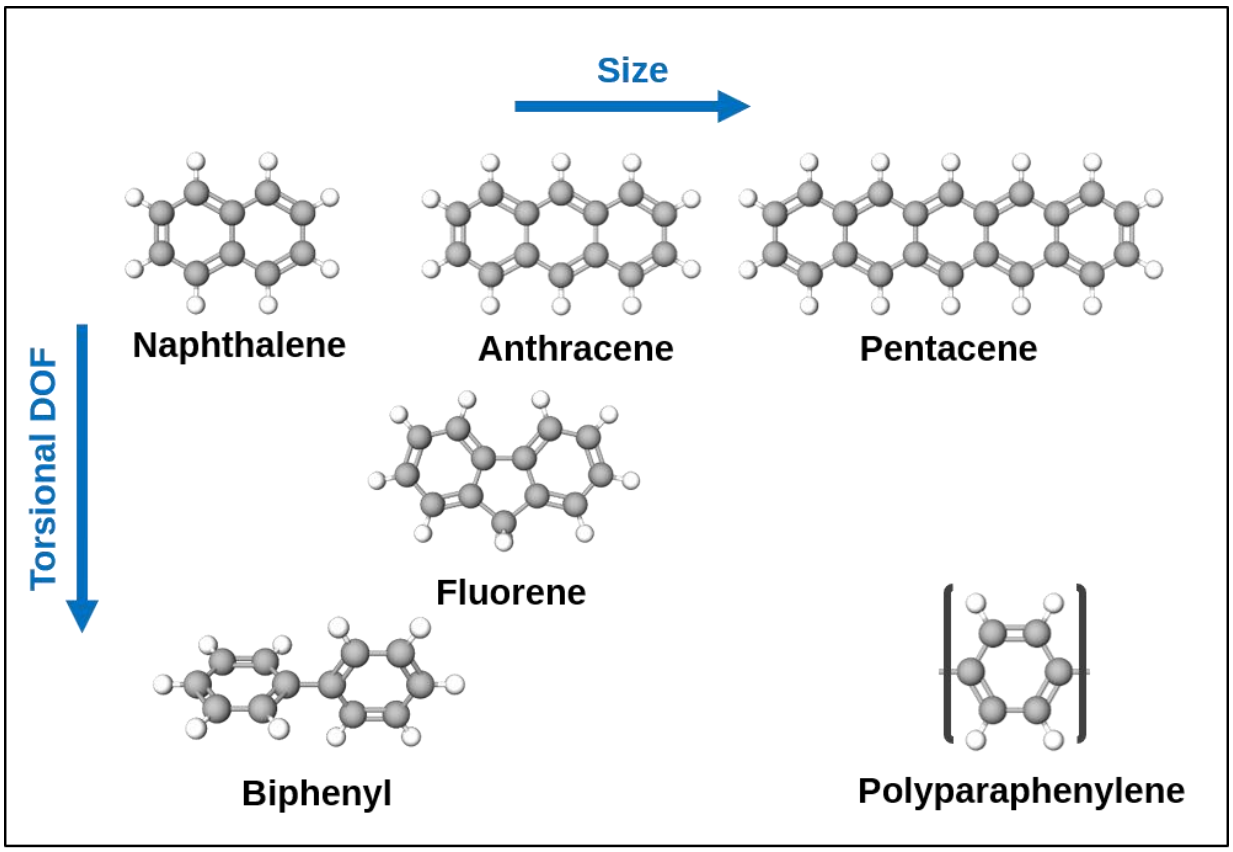

Figure 1: Materials under investigation, arranged to illustrate the variation in size (hor.) and torsional degree of freedom (vert.). Pictures were created using MolView[14]

Modeling Approach

The first step towards answering the aforementioned research questions is the choice of a suitable modeling methodology. This task always involves finding a balance between accuracy and computational effort, keeping in mind, that the computational resources are not unlimited. Specific to this work, the modeling method must be capable of calculating the full thermal conductivity tensor in order to investigate anisotropic behavior. Common theoretical methods to obtain thermal conductivity are based either on molecular dynamics or lattice dynamics or on a combination of both.[15] Among these approaches, the Green-Kubo[16,17] method (GK) and the non-equilibrium molecular dynamics (NEMD) are the most popular methods. The basis of the GK method is the general fluctuation-dissipation theorem by Kubo[18] which allows to relate the thermal conductivity to the time required for instantaneous fluctuations in temperature to dissipate. In NEMD

simulations, the thermal conductivity is calculated from the ratio of a heat flux to a temperature gradient. Usually, the system is subjected to a heat flux, by adjusting the velocity of atoms in distinct hot and cold segments of the simulation cell.[19,20] A temperature gradient will establish between those segments and once a steady-state is reached, thermal conductivity can be obtained from Fourier's Law. Although this method is very intuitive, the result has to be converged with respect to the geometry of the simulation cell, namely the number of segments, respectively their size and the cross section of the simulation cell. Because Fourier's Law is only applicable for linear response thermal conductivity must also be converged with respect to the magnitude of the applied heat flux. Unless the simulation cell is many times larger than the mean free path of phonons, the result has to be extrapolated to avoid finite-size effects.[21] The problem of finite-size effects is also important for GK calculations and therefore has to be addressed. As a main advantage of the GK method over NEMD simulations the whole thermal conductivity tensor can be obtained from one simulation whereas the other approach can solve Fourier's Law only in one dimension at once. However, GK calculations often require long simulation times to converge the correlation function to zero. Another common limitation to all molecular dynamics simulations is the treatment of atomic motion in terms of classical mechanics. Even if forces on atoms are obtained from first-principles calculations, atomic motion is calculated using Newton's equations of motion. This can cause errors at low temperatures as a consequence of quantum effects.[15]

Contrary to molecular dynamics, in lattice dynamics quantum effects are considered. The concept of lattice dynamics is used to calculate phonon properties which can be related to the thermal conductivity through the Boltzmann transport equation. For this approach the phonon frequencies with respect to momentum, i.e. the dispersion relation and the phonon lifetimes are required. The phonon dispersion relation is commonly obtained within the harmonic approximation, using either the concept of small displacements in real space[22] or perturbation theory.[23] A downside of this approximation is the fact, that phonons are considered decoupled and therefore don't interact.[24] Consequently, the phonon lifetime within the harmonic approximation is infinite and has to be obtained in a different way. A possible overcoming is the use of additional molecular dynamics simulations to estimate the lifetimes.[24,25] Another approach is anharmonic lattice dynamics, where phonon interactions are introduced as a perturbation to the harmonic solution to calculate the phonon lifetimes.[24,26] However, this method requires a large computational effort which limits its applicability to small systems. As a computationally cheaper alternative also empirical models are used to estimate the phonon lifetime.[27,28]

For the purpose of finding relations between the structure of molecular crystals and their ability to transport heat, the concept of lattice dynamics seems to be more promising. This approach allows to analyze the ingredients required for the Boltzman transport equation individually. Possible bottlenecks to thermal transport can therefore be identified and related to the structure of the molecular crystal.

The following work is structured into four chapters. In chapter 2, necessary theory to obtain the thermal conductivity is summarized starting with the derivation of the thermal conductivity tensor from the Boltzmann transport equation. Subsequently, lattice dynamics as well as the applied phonon lifetime model are explained in detail. The last part in this chapter then briefly introduces the applied quantum mechanical simulation tools, namely DFT and DFTB and the correction methods to account for van der Waals interactions accurately. To allow for reproducibility, chapter 3 focuses on the applied workflow, providing input parameters and other computational details. The findings of this work are then presented in chapter 4, followed by a concluding discussion of the most important results in chapter 5.

2. Theory

This chapter is intended to derive the expression for the thermal conductivity tensor within the chosen lattice dynamics approach. Subsequently, the ingredients to this equation are discussed, starting with harmonic quantities from lattice dynamics and then proceeding with anharmonic contribution in form of the phonon lifetime. Finally, this chapter will close with a brief introduction into first-principle simulations that were used in this work.

2.1. Thermal Conductivity Tensor

The following derivation of the thermal conductivity tensor is adapted from Festkörperphysik by Gross and Marx.[29] It will be shown in detail how the BTE can be used to model phononic heat transport using the RTA.

A crystalline solid, containing N atoms in its unit cell has 3N vibrational eigenmodes, which can be thermally occupied by phonons according to the Bose-Einstein-distribution:

$$f = \frac{1}{e^{\hbar\omega/k_B T} - 1} \tag{2.1}$$

The average phonon occupation of an eigenmode depends on the eigenmode's frequency and the temperature T. (cf. Figure 2 (left)) If an extended solid at an average temperature T^0 is now subjected to a temperature gradient, the local phonon occupation will deviate from the previous equilibrium one $f^0=f(T^0)$. At this point it should be emphasized, that the temperature gradient must be small enough, to allow for the assumption of constant temperature in a large enough region and, therefore, the use of statistics like the Bose-Einstein-distribution to characterize the phonon occupation in this region. Temperature deviation in neighboring regions relates to a deviation in phonon occupation, hence the phonon occupation is spatially dependent. In the first step towards thermal conductivity, the thermal flux will be expressed in terms of phonon properties. The general expression for the i^{th} component of the heat flux reads

$$j_i = \frac{1}{V}\sum_{q,n} \hbar\omega f v_{g,i} \tag{2.2}$$

with $v_g = \partial\omega/\partial q$, the phonon group velocity. For better readability, here and in the following equations, the indices of wavevector q and phonon band n, for ω, f and v_g are omitted. In thermal equilibrium with $\nabla T = 0$, heat flux vanishes because of identical phonon occupation for positive

and negative q-values, as well as the fact, that the dispersion relation is symmetric, hence $v_{g,i}(q) = -v_{g,i}(-q)$ and therefore the overall sum equals 0. In turn, a finite flux of heat establishes only, if f deviates from f^0:

$$j_i = \frac{1}{V}\sum_{q,n} \hbar\omega(f - f^0)v_{g,i} \tag{2.3}$$

There are two reasons for a deviation in phonon occupation. The diffusion of phonon can be imbalanced, meaning that more phonons diffuse towards a region than away from it. Furthermore, the phonon occupation is altered by all kinds of interactions amongst colliding phonons. For the considered stationary case, the overall phonon occupation doesn't change, hence $\frac{df}{dt} = 0$, thus, the BTE for no external forces reads:

$$\left.\frac{\partial f}{\partial t}\right|_{diff.} = \left.\frac{\partial f}{\partial t}\right|_{coll} \tag{2.4}$$

The diffusion term on the left-hand side represents a system of noninteracting phonons. All possible mechanisms of interactions amongst phonons are accounted for in the right-hand side collision term.[24] The diffusion of phonons is of course related to the phonon occupation, which depends on temperature. Therefore, the diffusion term must be related to the temperature gradient. Within the period Δt, all phonons will have traveled from their initial position $x - v_g\Delta t$ to position x, the diffusion term can therefore be written as:

$$\left.\frac{\partial f}{\partial t}\right|_{diff.} = \lim_{\Delta t\to 0}\frac{1}{\Delta t}\left[f\left(x - v_g\Delta t\right) - f(x)\right] = -v_g\frac{\partial f}{\partial x} = -v_g\frac{\partial f^0}{\partial T}\frac{\partial T}{\partial x} \tag{2.5}$$

The fluctuations of the distribution function are assumed to be independent of temperature and thus the equilibrium distribution f^0 can be considered instead of the local distribution f. The second source for changes in phonon occupation is scattering. Describing the interaction of particles thoroughly can be a difficult task, thus simplifications are necessary. In the relaxation time approximation, the collision term is considered to have the form:

$$\left.\frac{\partial f}{\partial t}\right|_{coll.} = -\frac{f - f^0}{\tau} \tag{2.6}$$

A deviation in phonon occupation is restored to equilibrium within a relaxation time τ. The collision terms magnitude, or in other words, the collision rate is proportional to the deviation in phonon occupation.

Equations (*2.5*) and (*2.6*) can now be inserted into equation (*2.3*) which can then be compared to Fourier's Law (cf. eq. (*1.1*)) to obtain the final equality, written in a general form with v_g instead of v_x:

$$\kappa = \frac{1}{V}\sum_{q,n} \hbar\omega \frac{\partial f^0}{\partial T} v_g^2 \nabla T \tau \tag{2.7}$$

Finally, the specific heat can be expressed as the sum of phonon mode heat capacity, in the form:

$$C_V(T) = \frac{1}{V}\sum_{q,n} \hbar\omega \frac{\partial f^0}{\partial T} = \frac{1}{V}\sum_{q,n} C_{ph}(q,n) \tag{2.8}$$

and identified in equation (*2.7*). For isotropic materials, thermal conductivity is a scalar, however, in most cases anisotropy plays a role and the thermal conductivity is represented as tensor κ_{ij}. With this final step of identifying the mode heat capacity the thermal conductivity tensor derived using the BTE within the RTA reads as:

$$\kappa_{ij} = \frac{1}{V}\sum_{q,n} C_{ph}(q,n) v_{g,n,i}(q)\, v_{g,n,j}(q) \tau_n(q) \tag{2.9}$$

The phonon mode heat capacity $C_{ph}(q,n)$ is the heat capacity contribution of one phonon mode, integrated over all frequencies it represents the phononic contribution to specific heat $C_V(T)$. In the expression of κ, C_{ph} is the only temperature dependent part, acting as a filter function for phonon modes to contribute to thermal conductivity. Figure 2 illustrates the shape of this function, showing the frequency range for given temperatures. For comparison, also the Bose-Einstein distribution (cf. equ. (*2.1*)) is displayed along with the general univariate function for the phonon mode heat capacity, which is much broader than the occupation function.

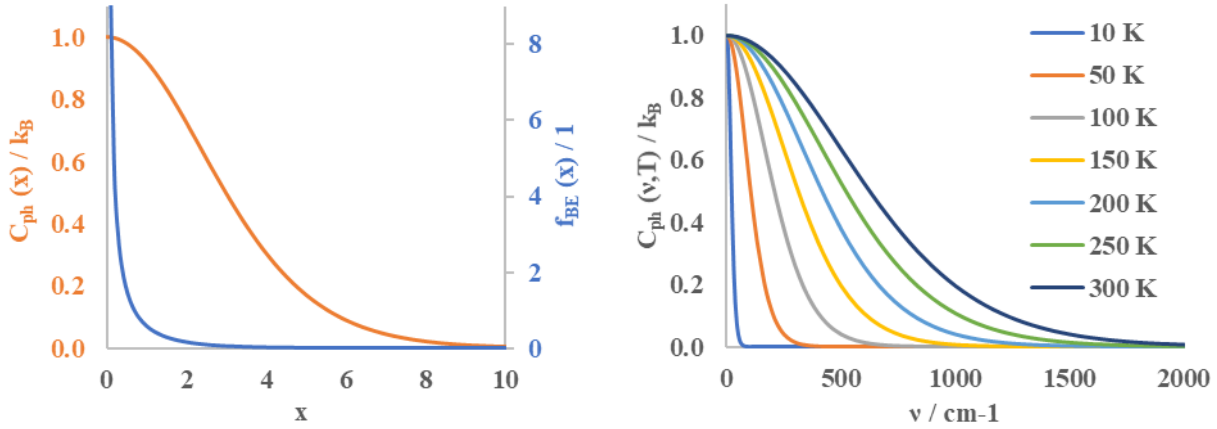

*Figure 2: Bose-Einstein distribution compared to the heat capacity function (cf. equ. (*2.8*)) in dependence of* $x = \hbar\omega/k_B T$ *(left) and the phonon mode heat capacities for different temperatures (right).*

The ingredients necessary to calculate thermal conductivity from equ. (*2.9*) are the phonon band structure and the mode dependent relaxation times. The band structure provides wavevector dependent frequencies to calculate phonon mode heat capacities C_{ph}. The group velocity v_g is extracted as the first derivative with respect to the wavevector:

$$v_{g,n,i}(q) = \frac{\partial \omega_n(q)}{\partial q_i} \qquad (2.10)$$

In this work, the relaxation time is obtained from a phonon lifetime model, which will be discussed subsequently to the following section on harmonic lattice dynamics.

2.2.Harmonic Lattice Dynamics

Now that it has become clear what ingredients are necessary to calculate the thermal conductivity this section aims for a brief introduction on how to obtain the phonon dispersion relation, which provides two ingredients to thermal conductivity, the frequencies for the phonon mode heat capacities and the group velocities. To describe vibrations within a crystal, Newton's equations of motion need to be solved for all atoms in the crystal.[30] For a complex system with many atoms, this turns out to be a difficult task, thus approximations are necessary to simplify the procedure.

A common approach to obtain the phonon dispersion relation is the concept of harmonic lattice dynamics. The interaction between atoms in a crystal can be of great variety and, therefore, the interaction potential can have a complex shape. Within the harmonic approximation, one assumes the interaction between atoms to be modelled as linear springs and, therefore, the interaction potential to be of parabolic shape. It shall not be omitted, that this simplification only holds true

for small deviations of the atom's position around its equilibrium position. At room temperature, atoms' displacements can be of the order of 10% of the lattice parameter.[29] Consequently, the results obtained within harmonic approximation will show deviations at elevated temperatures.

In the first step, the potential energy is Taylor expanded at its minimum with respect to the displacement $u_i^a(A)$ of atom a in unit cell A towards cartesian direction i:

$$E(r+u) = E(r) + \sum_a \sum_i \sum_A \left.\frac{\partial E}{\partial u_i^a(A)}\right|_r u_i^a(A) + \frac{1}{2}\sum_{a,b}\sum_{i,j}\sum_{A,B} \left.\frac{\partial^2 E}{\partial u_i^a(A)\partial u_j^b(B)}\right|_r u_i^a(A)u_j^b(B) \ldots \quad (2.11)$$

The 0th oder term represents the ground state energy which can be omitted for further discussion. The first derivative of energy with respect to a displacement is nothing else than the sum of forces acting on atom a. By the definition of equilibrium, those forces have to vanish and so does this term. In the harmonic approximation, the Taylor expansion is cut off after the second derivatives, and one obtains the harmonic potential. The second derivatives of the harmonic potential are referred to as force constants and relate the forces acting on atom a in unit cell A towards direction i upon displacement of atom b in unit cell B towards direction j:

$$C_{ij}^{ab}(A,B) = \frac{\partial^2 E}{\partial u_i^a(A)\partial u_j^b(B)} = -\frac{\partial F_j^b(B)}{\partial u_i^a(A)} \quad (2.12)$$

The second equality represents the force F exerted on atom b in unit cell B towards direction j upon displacement of atom a in unit cell A towards direction i. The force constants must satisfy several requirements which arise from the isotropy of space and the point group symmetry. Due to translational invariance in a periodic structure, the interatomic force constants are only dependent on the difference between the unit cells. In other words, it is not necessary to have two indices A and B running over all possible unit cells. Instead a central unit cell 0 can be defined and the summation of interactions is performed for all periodic repetitions, B. Therefore, the force constants can be rewritten as:

$$C_{ij}^{ab}(A,B) = C_{ij}^{ab}(0,B) \quad (2.13)$$

To obtain now the relation between the frequency and the wavevector of a phonon, the laws of classical mechanics can be applied. According to Newton, the forces upon interaction are in balance

with the inertial forces. To reduce the size of the resulting system of equations, the periodicity of the system can be utilized to apply a plane wave ansatz for the atoms' displacements, similar to Bloch's theorem:

$$u_i^a(A) = \frac{1}{\sqrt{m_a}} \lambda_i^a(q) e^{i(qR_A - wt)} \tag{2.14}$$

Here m_a is the mass of atom a and λ_i^a is the amplitude of the plane wave. In contrast to general plane waves, this one is only defined at the lattice points R_a. This ansatz is now inserted into Newton's equations of motion to obtain a homogeneous system of linear equations. To solve this system, the so-called dynamical matrix D needs to be diagonalized. The entries of the dynamical matrix are of the form:

$$D_{ij}^{ab}(q) = \frac{1}{\sqrt{m_a m_b}} \sum_B C_{ij}^{ab}(0, B) e^{-iqR_B} \tag{2.15}$$

The components of this matrix are the Fourier transform of all force constants between two atoms normalized by their masses. A crucial step in this approach is to converge the sum in equation (*2.15*) by considering a supercell, large enough for the present interactions to decay. Thus, force constants have decayed as well ensuring converging entries to the dynamical matrix. The phonon frequencies $\omega_n(q)$ and eigenvectors $e_n(q)$ can then be obtained for any wavevector q:

$$\omega_n^2(q) = e_n(q)^T D(q) e_n(q) \tag{2.16}$$

For badly converged force constants, the dynamical matrix can contain complex entries which in turn results in phonons of negative frequency, and therefore also negative energy. This is of course physically meaningless.

2.3. Computation of Force Constants – FDM

To compute force constants, the derivative of the energy with respect to the displacement of an atom is required. Within the method of finite differences, equation (*2.12*) can be used to obtain the finite difference quotient as an approximation to the real derivative. Every single atom in the central unit cell is displaced six times, towards all three cartesian directions for a positive and a negative increment (+/- x, +/-y, +/-z). In a system without any symmetries, 6N different displacement setups would be necessary to be calculated. In return, the symmetries inherent to the investigated systems decrease the computational effort, e.g. with 36 atoms in the unit cell, Naphthalene would require

216 different displacement setups, whereas considering symmetries the number of displacements is decreased to a 54. For every displacement setup with one atom being displaced, the occurring forces on all other atoms are calculated and the according force constants can be obtained.

One crucial parameter of this approach is the magnitude of the atom displacement. The displacement must be small enough to stay within harmonic approximation whereas too small displacements would cause nothing else than numerical noise. For all investigated materials, the displacement was set to be 0.01Å, which is less than one percent of the usual bond distances of around 1-2Å.

2.4.Phonon Lifetime Model

Having discussed how the harmonic ingredients to thermal conductivity are obtained, this section focuses on the anharmonic contribution in the form of phonon lifetimes. In the harmonic approximation, phonons have an infinite lifetime because no interaction between phonons can be modelled. In real materials however, phonons can scatter with each other or at defects, impurities, grain boundaries and other interfaces. All those effects cannot be modelled without consideration of higher order terms of the potential energy. A straightforward idea would, therefore, be, not to use the harmonic approximation in which the Taylor expansion of the potential energy is truncated after the second order term, but rather to include at least the third order term. Applying Fermi's golden rule then allows to calculate the phonon lifetimes analytically. However, compared to the second order force constants that were obtained by displacing one atom and calculating the occurring forces, third order force constants require the displacement of two atoms simultaneously. In return, the number of different displacement setups increases dramatically even after consideration of symmetries. Sticking again to Naphthalene as an example, the second order force constants require 54 different displacements, whereas the third order force constants need more than 90.000 different setups to be calculated.

Due to the massive computational effort, this approach was dismissed in the present work. As an alternative, a phonon lifetime model was employed which was published by Bjerg et al.[31]. This model relies on the Grüneisen parameters as a measure for the internal anharmonicity. Before a further discussion of the phonon lifetime model, first the mode dependent Grüneisen parameter $\gamma_n(q)$ and then the mean squared Grüneisen parameter $\langle\gamma^2\rangle$ will be explained briefly. The mode dependent Grüneisen parameter characterizes the relative change in phonon frequency $\omega_n(q)$ upon a change, either contraction or expansion, of the equilibrium volume V_0 of the unit cell:

$$\gamma_n(q) = -\frac{V_0}{\omega_n(q)}\frac{\partial \omega_n(q)}{\partial V}\bigg|_{V_0} = -\frac{V_0}{2\omega_n(q)}\langle e_n(q)|M(q)|e_n(q)\rangle \qquad (2.17)$$

$$M(q) = \frac{\partial D(q)}{\partial V}\bigg|_{V_0} \approx \frac{\Delta D(q)}{\Delta V}\bigg|_{V_0} \qquad (2.18)$$

The first equality in equation (*2.17*) is the definition of the mode dependent Grüneisen parameter and the second equality is the way how the mode dependent Grüneisen parameters were calculated in this work. The dynamical Matrix (cf. equ. (*2.15*)) is obtained for three different volumes to construct a new matrix M (*2.18*), instead of calculating the frequency change for every mode at each desired q-point.

Its use as measure of anharmonicity arises from the fact, that for a perfectly harmonic potential energy, the phonon frequencies would not depend on the volume of the unit cell and the Grüneisen parameters would vanish. Also, the Grüneisen parameters can approximately be related to the third derivatives of the potential energy as the phonon frequency is proportional to energy and $\partial V = \partial x \partial y \partial z$.

The mean squared Grüneisen parameter is the averaged Grüneisen parameter, weighted by the phonon mode heat capacity. To prevent the cancelation of positive and negative Grüneisen parameters, they are squared:

$$\langle \gamma^2 \rangle = \frac{\sum_{n,q} C_{ph}(n,q)\big(\gamma_n(q)\big)^2}{\sum_{n,q} C_{ph}(n,q)} \qquad (2.19)$$

The present phonon lifetime model is obtained by comparing two earlier lifetime models considering a Debye model with three acoustic branches having the same speed of sound, relaxation time and Debye temperature. One model, proposed by Slack[28], is based on the empirical finding for the relaxation time around the Debye temperature for the case of dominant three phonon scattering:

$$\tau_n^{-1}(q) = p(\langle \gamma^2 \rangle)\, \omega_n^2(q) \frac{T}{\Theta} e^{-\Theta/3T} \qquad (2.20)$$

The components of this equation are, $p(\langle \gamma^2 \rangle)$, an empirical fit function which depends on the mean squared Grüneisen parameter, the squared phonon frequency $\omega_n^2(q)$ with band index n and

wavevector q. T denotes the temperature and Θ is a temperature scaling factor which corresponds to the Debye temperature for inorganic materials.

A second model, also by Slack et al.[32], based on the work of Leibfried and Schlömann for the thermal conductivity in noble gas crystals[33] was compared to the thermal conductivity according to equation (*2.9*) within the Debye model to obtain the fitting function p:

$$p = \frac{1 - 0.514(\langle\gamma^2\rangle)^{-1} + 0.228(\langle\gamma^2\rangle)^{-1}}{0.0948} \frac{\hbar^2\langle\gamma^2\rangle}{k_B\Theta M V^{1/3} s} \qquad (2.21)$$

Here M denotes the average atomic mass in the unit cell, V is the unit cell volume and the speed of sound is represented by s. In this work, the temperature scaling factor was calculated from the second moment of the phonon density of states:

$$\Theta = \sqrt{\frac{5\hbar^2 \int_0^{\nu_{cut}} \omega^2 g(\omega) d\omega}{3k_B^2 \int_0^{\nu_{cut}} g(\omega) d\omega}} \qquad (2.22)$$

In their work, Bjerg et al. employed an additional scaling factor $N^{-1/3}$ to scale equation (*2.22*), with N the number of atoms in the unit cell. In contrast to the methodology proposed by Bjerg et al., the integral in equation (*2.22*) was truncated to a cutoff frequency ν_{cut}, which was defined as the maximum frequency of any of the acoustic bands. This choice is justified by the assumption, that the acoustic phonons are the main contributors to thermal transport.[32]

According to the authors, the strengths of the lifetime model are, that the full phonon dispersion is considered, and no further fitting parameters are necessary. The second point is only partially complied as the model is based on earlier empirical models that do feature already determined fitting parameters which therefore also enter the present model, however, they were not changed or refitted within this thesis. One drawback of the used lifetime model is the simplified assumption of one generalized phonon lifetime which only depends on frequency. Due to the lack of directional dependence in this applied phonon lifetime model, anisotropy of the calculated thermal conductivities stems solely from the group velocities, which should be noted when discussing the results of this work.

2.5. Quantum Mechanical Simulation Software

As outlined in the previous section on lattice dynamics, the main ingredient required to calculate the phonon band structure are the forces acting on an atom while its position deviates from the

equilibrium position to a known extend. Within this work, quantum mechanical simulation software was used to perform total energy calculations, as the gradient of the total energy with respect to an atom's position equals the force acting on the atom. Software tools used are based in density functional theory (DFT) and density-functional tight-binding theory (DFTB). Due to the importance of vdWs interactions for molecular crystals, additional correction-methods were applied in the form of the Tkatchenko-Scheffler method[34] and the dispersion correction by Grimme et al. termed D3[35]. In the following, the basics of those methods are discussed, starting with the foundations of DFT by showing the theorems of Hohenberg and Kohn and the Kohn-Sham equations, also mentioning functionals. The subsequent section then serves the purpose of briefly introducing the density-functional tight-binding formulism. The last subsection then is dedicated to the applied vdWs corrections.

2.5.1. Density Functional Theory

To obtain the total energy of a system of atoms one has to solve the Schrödinger equation. For a system containing N electrons, solving the Schrödinger equation is a 3N dimensional many-body problem.[36] In the mid 1960's, Hohenberg and Kohn[37] could show, that the ground state energy is a unique functional of the electron density n(r), or in other words, the ground state wave function directly corresponds to the ground state electron density. Important about this finding is, that the electron density is a function in three dimensions only, compared to the 3N dimensionality of the Schrödinger equation. Furthermore, they could prove, that the true electron density corresponding to the solution of the Schrödinger equation is the one, which minimizes the energy functional. Further development by Kohn and Sham (KS) then led to a first framework of DFT, where the problem of solving Schrödinger's equation is mapped onto an auxiliary system of noninteracting electrons affected by an effective potential. They suggested an energy functional of the form:

$$E_{KS} = T_S[n(\boldsymbol{r})] + \int V(\boldsymbol{r})n(\boldsymbol{r})d\boldsymbol{r} + \frac{1}{2}\int \frac{n(\boldsymbol{r})n(\boldsymbol{r}')}{|\boldsymbol{r}-\boldsymbol{r}'|}d\boldsymbol{r}d\boldsymbol{r}' + E_{XC}[n(\boldsymbol{r})] \qquad (2.23)$$

where T_S is the kinetic energy of a system of non-interacting electrons, V(r) is the external potential arising from the positively charged nuclei and the third term represents the Coulomb interaction between pairs of electrons, also denoted as Hartree potential $V_H(r)$.[36] The term E_{XC}, which characterizes the exchange and correlation energy, contains all quantum mechanical, many-body and self-interaction effects, which are not included in the other terms. In theory, if one could find an analytical description for the exchange-correlation energy, one could find the exact solution to

equation (*2.23*), however the true form of the exchange-correlation functional is not known and has to be approximated.[38]

To find now the right electron density, Kohn and Sham[39] could further demonstrate, that one simply has to solve one-particle Schrödinger equations of the form,

$$\left[-\frac{\hbar^2}{2m}\nabla^2 + V(\boldsymbol{r}) + V_H(\boldsymbol{r}) + \frac{\partial E_{XC}[n(\boldsymbol{r})]}{\partial n(\boldsymbol{r})}\right]\psi_i(\boldsymbol{r}) = \epsilon_i\psi_i(\boldsymbol{r}) \qquad (2.24)$$

where ψ_i denotes the KS-orbitals. The electron density can then be calculated by summation of the occupied KS-orbitals:

$$n(\boldsymbol{r}) = \sum_i^N \psi_i^*(\boldsymbol{r})\psi_i(\boldsymbol{r}) \qquad (2.25)$$

This scheme can now be solved in a self-consistent manner, called self-consistent-field (SCF) approach. First, an initial electron density n(r) is guessed which is used to calculate the effective potential to then solve the KS-equations. Now the actual electron density can be computed and compared to the initial guess. In case the two densities differ, the initial guess is updated, and the KS-equations are again solved. This cycle is repeated until the electron densities converge. If convergence was reached, the resulting electron density is the ground state electron density which can then be used to calculate the total energy.

The last missing ingredient to this approach is the treatment of the exchange and correlation energy, the exchange-correlation functional. In their paper from 1965, Kohn and Sham used the so-called local density approximation (LDA) which relates this energy to the energy within a uniform electron gas of density n(r):

$$E_{XC}^{LDA} = \int d\boldsymbol{r}\, n(\boldsymbol{r})\epsilon_{XC}[n(\boldsymbol{r})] \qquad (2.26)$$

Another type of approximation for the exchange-correlation energy additionally considers the gradient of the electron density, hence this type of functionals is called generalized gradient approximation, GGA. The functional used within this work, the PBE functional, proposed by Perdew, Burke and Ernzerhof, also belongs to the family of GGA's.[40]

2.5.2. Density-Functional Tight-Binding

For calculation of force constants, the Fourier series in equation (*2.15*) must converge, which requires super cells large enough for the occurring forces to decay. The computational costs to perform DFT calculations on such large super cells, that are built from already large unit cells, concerning the number of atoms, were too high for some materials and denied the use of DFT. As an alternative, density-functional tight-binding theory (DFTB) was applied. This method has shown reasonable accuracy compared to DFT[41,42] with much lower computational expenses. Therefore, this approach is very well suited to study large systems. In this work the free software DFTB+[43] was used, which is an implementation of the DFTB method. Currently, three evolutions of DFTB are available, the non-self-consistent DFTB1[44], the second-order DFTB2[45], which was originally referred to as SCC-DFTB and the most recent DFTB3[46] which is an extension to the third-order. In the following, the basics of DFTB are derived, however, only up to the second-order extension. The derivation is adapted from an article by Elstner and Seifert[47], where the basic principles of DFTB are reviewed.

Instead of the electron density as the main quantity, for DFTB a reference density n^0 is assumed, perturbed by a density fluctuation δn: $n(\boldsymbol{r}) = n^0(\boldsymbol{r}) + \delta n(\boldsymbol{r})$. Inserting this into the KS-equations and after expansion of the exchange-correlation energy functional up to the third order, the total energy reads:

$$\begin{aligned} E^{DFTB3}[n^0+\delta n] &= \frac{1}{2}\sum_{ab}\frac{Z_a Z_b}{R_{ab}} - \frac{1}{2}\iint\frac{n^0(r)n^0(r')}{|r-r'|}drdr' \\ &\quad - \int V^{XC}[n^0]n^0(r)dr + E^{XC}[n^0] + \sum_i n_i\langle\psi_i|\hat{H}[n^0]|\psi_i\rangle \\ &\quad + \frac{1}{2}\iint\left(\frac{1}{|r-r'|} + \left.\frac{\delta^2 E^{XC}[n]}{\delta n(r)\delta n(r')}\right|_{n^0}\right)\delta n(r)\delta n(r')drdr' \\ &\quad + \frac{1}{6}\iiint\left.\frac{\delta^3 E^{XC}[n]}{\delta n(r)\delta n(r')\delta n(r'')}\right|_{n^0}\delta n(r)\delta n(r')\delta n(r'')drdr'dr'' \\ &= E^0[n^0] + E^1[n^0,\delta n] + E^2[n^0,(\delta n)^2] + E^3[n^0,(\delta n)^3] \end{aligned} \tag{2.27}$$

The evolutions of DFTB mentioned above differ in the contributing terms and build up on top of each other in a successive manner. For the non-self-consistent DFTB1 method, the first two terms of equation XX, $E^0[n^0]$ and $E^1[n^0,\delta n]$ are considered. As a basis of the DFTB approach, the KS-

orbitals are constructed form the linear combination of atomic orbitals (LCAO) where the atomic orbitals are obtained from DFT calculations:

$$\psi_i = \sum_{\mu} c_{\mu i} \psi_{\mu} \tag{2.28}$$

A minimal basis set restricted to the valence shell of the atoms is used, which requires an orthogonalization to the atoms core orbitals. As a consequence of the LCAO ansatz the general eigenvalue problem arises

$$\sum_{v} c_{vi}\left(H^0_{\mu v} - \epsilon_i S_{\mu v}\right) = 0 \quad with\ v \in b\ and\ \forall a, \mu \in a \tag{2.29}$$

where $H^0_{\mu v}$ are the elements of the Hamiltonian matrix and $S_{\mu v}$ are the elements of the overlap matrix, and a and b denote the different atoms. The Hamiltonian matrix elements are obtained within a two-center approximation directly from DFT calculations. According to[47], pure atomic orbitals would be too diffuse for the chosen minimal basis set, hence an additional harmonic potential is applied for solving the atomic KS-equations, which results in *'compressed'* atomic orbitals. For this reason, a confinement radius r0 has to be provided, which is usually chosen to be double the covalent radius of the atom.[44] Also the electron density of the neutral atom is obtained in this way, therefore a confinement radius for the initial density r_0^d has to be specified. Those two parameters have to obtained for every element. Having determined the atomic orbital basis and the initial density, the KS-equations can be solved leading to the electronic energy of the DFTB model

$$E^1 = \sum_i n_i \sum_{\mu v} c^i_{\mu} c^i_{v} H^0_{\mu v} = \sum_i n_i \epsilon_i \tag{2.30}$$

which equals the sum of occupied KS energies with n_i representing the occupation number of KS orbital i. To determine the total energy, the term $E^0[n^0]$ must be defined. Considering equation (*2.27*), this term accounts for the 'double-counting' in DFT and solely depends on the reference density n^0, obtained from the superposition of neutral atomic densities. This implies, that E^0 does not depend on the chemical environment, thus it can be obtained beforehand without limiting the transferability of the parameter. In DFTB, E^0 is referred to as repulsive energy term and approximated by summing over pair potentials, determined either by comparing to DFT calculations or empirical data. Finally, the total energy of the non-self-consistent DFTB1 reads:

$$E^{DFTB1} = \sum_i n_i \epsilon_i + \frac{1}{2} \sum_{ab} V_{ab}^{rep} \qquad (2.31)$$

DFTB1 is a very efficient method, due to the use of a minimal basis set and furthermore, because the Hamilton matrix elements as well as the overlap matrix elements are precalculated and stored in so called Slater-Koster-files and don't require calculation during the runtime. Additionally, the KS equations need to be solved once as this approach is non-self-consistent. Although many approximations are made within this method, it is still very well suited for systems with negligible charge transfer.

For systems where charge transfer does play a role, the accuracy of DFTB1 is of course limited, which can only be omitted by using higher order terms of equation (*2.27*) and solving them iteratively. To start with, the density fluctuations δn are expressed as superposition of atomic contributions and the atomic-like density fluctuations undergo a multipole expansion, of which only the monopole term is kept. For evaluation of the second-order integral in equation (*2.27*), the charge density is modelled to decay exponentially. Finally, the second-order term can be stated

$$E^2 = \frac{1}{2} \sum_{ab} \Delta q_a \Delta q_b \gamma_{ab} \qquad (2.32)$$

where Δq_a denotes the partial charge at atom a and function γ_{ab} takes care of the Coulomb and exchange-correlation interactions. Now the Hamilton matrix elements depend on the partial charges at the atoms, which in turn depend on the expansion coefficients of the LCAO ansatz. These equations require an iterative evaluation and the method is also called self-consistent-charge DFTB (SCC-DFTB).

2.5.3. Van der Waals corrections

Although much weaker than covalent bonds, van der Waals (vdW) interactions play an important role in molecular crystals. They are essential for the formation of organic solids and have a great effect on the crystal structure.[48] Consequently, also properties that depend on the crystal structure, e.g. the phonon band structure we are interested in, are affected by the correct description of those interactions. Sadly, neither DFT nor DFTB account for dispersion interactions right away, however, there are several approaches to overcome this issue.[34,35,49] In this work, two vdW corrections were used, TS and D3, and both are so called DFT-D approaches, where a dispersion energy contribution E_{DISP} is added to the total energy E_{DFT}:

$$E_{DFT-D} = E_{DFT} - E_{DISP} \tag{2.33}$$

The dispersion energy is the sum of two-, in D3 also three-body energies. For pairwise interactions, this term is generally of the form

$$E_{DISP} = s \sum_{AB} \frac{C_{AB}^6}{r_{AB}^6} f_{damp}(r_{AB}) \tag{2.34}$$

where r_{AB} is the distance between atoms A and B, C_{AB}^6 is a dispersion coefficient and $f_{damp}(r_{AB})$ is a damping function necessary to omit double counting effects of correlation and avoid singularities at small interatomic distances. A scaling factor s is used globally, to adjust E_{DISP} with respect to the used density functional. In the following, the two dispersion corrections will be discussed briefly.

In TS, the aim is put on obtaining effective dispersion coefficients to account for the chemical environment. The starting point is the Casimir-Polder integral, which is used to express the relation between atomic polarizabilities and the dispersion coefficient. From there, an expression for C_{AB}^6 is derived, which relies only on homonuclear parameters. To account then for the chemical environment, the effective volume of an atom in a molecule is defined, making use of the direct relation between volume and polarizability by applying the Hirshfeld partitioning of the electron density. The obtained effective volume can then be compared to the value for the free atom to obtain the effective dispersion coefficient. Intermolecular dispersion coefficients, C_{mol}^6, can be obtained from summation over all atomic dispersion coefficients. Within TS, a Fermi-type damping function is utilized

$$f_{damp}(r_{AB}, r_{AB}^0) = \frac{1}{1 + \exp[-d\left(\frac{r_{AB}}{s_R r_{AB}^0} - 1\right)]} \tag{2.35}$$

with $r_{AB}^0 = r_A^0 + r_B^0$ as the combined vdW radius. The steepness of the damping function is determined with parameter d, set to 20. Parameter s_R is used to adjust the onset in terms of distance of the vdW correction for a certain exchange-correlation functional. To define the vdW radius, Tkatchenko and Scheffler again use the ratio between the effective and the free atomic volume.

D3 also handles the description of vdW interactions in form of an additional energy contribution to the total energy of DFT, however, here also three-body terms are considered which will be

discussed shortly after showing how pairwise interactions are modelled. The first specialty of D3 is, that the scaling factor s (cf. equ. (*2.34*)) is set to unity in order to preserve an exact asymptotic behavior of the interactions. Because of the missing scaling factor, higher order terms of C_{AB}^{n} are required, which then can be scaled by s_n to fit the vdW correction to the used density functional. In D3, an additional eighth-order term is used. Higher order terms were omitted due to computational instability while at the same time, not improving the accuracy of the method. The C_{AB}^{6} are obtained from time-dependent DFT calculations solving the Casimir-Polder integral, whereas the higher order coefficients are obtained recursively. As a damping function, Grimme et al. choose an approach by Chai and Head-Gordon[50] which reads

$$f_{damp,n}(r_{AB}) = \frac{1}{1 + 6\left(\frac{r_{AB}}{s_{r,n} r_{AB}^{0}}\right)^{-\alpha_n}} \tag{2.36}$$

with $s_{r,n}$ representing the order-dependent scaling factor of the cutoff radii r_{AB}^{0}, which determines the adaptation at small and medium distances of the correction to the specific density functional. The steepness of this damping functions is adjusted with α_n, set to 14 for the sixth-order and 16 for eighth-order. The three-body term used in D3 is derived from third-order perturbation theory and reads

$$E_{ABC} = \frac{C_{ABC}^{9}(3\cos\theta_a \cos\theta_b \cos\theta_c + 1)}{(r_{AB} r_{BC} r_{CA})^3} \tag{2.37}$$

with θ_A, θ_b and θ_c denoting the internal angles of the triangle spanned by r_{AB}, r_{BC} and r_{CA}. C_{ABC}^{9} is the triple-dipole constant which could be obtained from the Casimir-Polder integral in analogy to the dipole coefficient, however, due to the low contribution to the dispersion energy (<5-10%) the coefficient is obtained as the geometric mean of the C^6-coefficients. Applying the analogous damping scheme as for the pairwise interactions completes the treatment of triple-dipole interactions. As a cutoff radius for both two- and three-body terms, the distance where the first-order DFT interaction energy between two atoms equals a certain cutoff energy is taken. To account for the chemical environment, which is changed e.g. by the formation of covalent bonds, an approach employing a fractional coordination number (CN) is used. Roughly speaking, the distance between two atoms is compared to the covalent bond distance of those two atoms to decide whether the atoms are bonded or not. This counting is performed for all atoms in the system to calculate the CN. The dispersion coefficient of an atom in its certain chemical environment can then be obtained

from an interpolation scheme between precalculated values for the pairs of atoms, which are calculated for different CN.

A recently published paper by Bedoya et al. shows, the importance of vdW correction methods to obtain vibrational properties comparable to experimental ones. Furthermore, it is shown, that the D3-method delivers a very accurate description of vdW interactions in molecular crystals concerning vibrational properties. However, it should also be mentioned, that for known lattice parameters, calculations using the PBE functional without any dispersion correction schemes also result in accurate vibrational properties.[51]

3. Workflow

After having discussed the theory relevant to this work in the previous chapter, the current chapter is intended to show the steps necessary to obtain the thermal conductivity tensor. Moreover, this chapter aims to provide detailed information about the used software tools, input parameters and settings. The workflow to achieve thermal conductivities is depicted in Figure 3 showing the main steps as well as the used software. In the first step, input parameters and settings must be converged

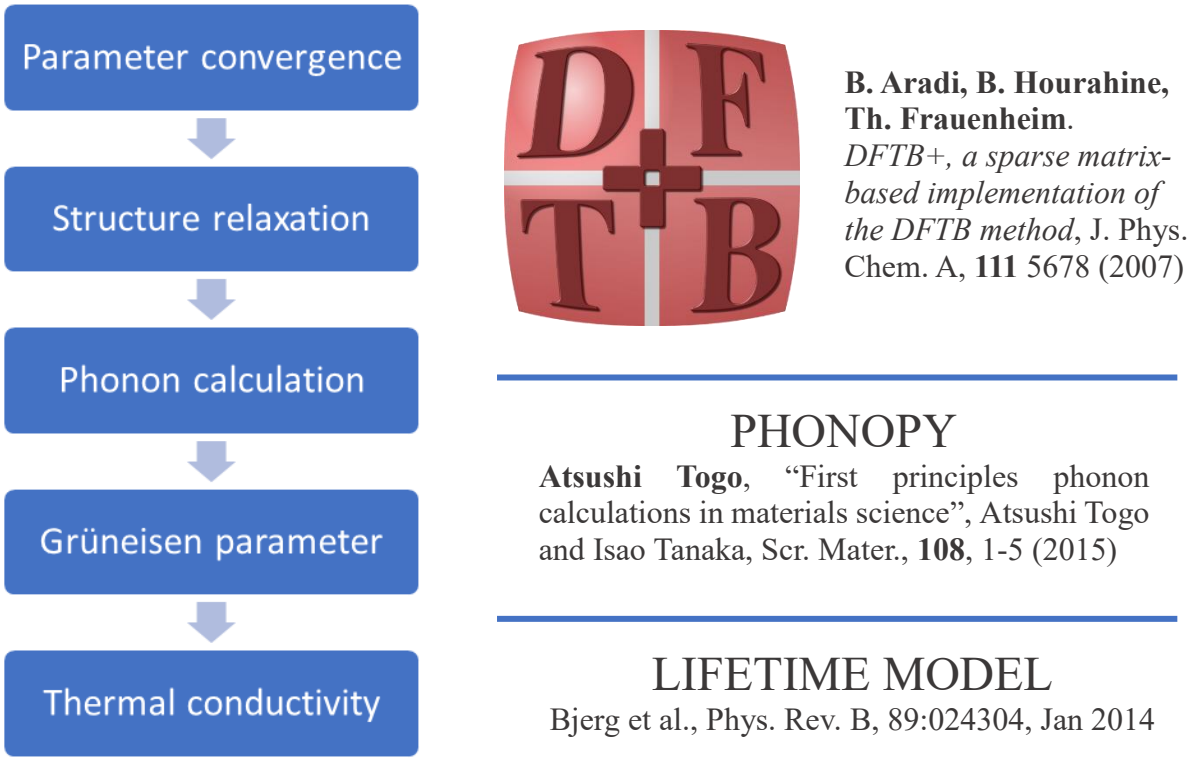

Figure 3: Flow chart illustrating the general workflow and the used software to obtain thermal conductivity.

to give meaningful results. One of the most important steps for harmonic lattice dynamics is structure relaxation, which contains both, the optimization of lattice parameters, as well as the relaxation of atom positions inside the crystal structure. Residual forces on atoms must vanish and the structure must be at a minimum of the potential energy to obtain meaningful phonon properties. For the subsequent step of phonon calculation, which contains the creation and handling of displacement setups, construction and diagonalization of the dynamical matrix, as well as the postprocessing to access the phonon properties, the open source package phonopy was employed. Phonopy was, furthermore, used for the calculation of Grüneisen parameters. Thermal conductivities were then obtained according to the discussed lifetime model.

Although there is only DFTB+ shown in Figure 3, total energy and force calculations for some materials were also performed with VASP, however, all results presented here were obtained using DFTB+. The reason to prefer DFTB+ over VASP will be explained in the first section of this chapter. Furthermore, a comparison of phonon properties obtained with both software packages is shown to confirm the quality of the more approximative tight-binding approach compared to DFT for the calculation of phonons. The second part of this chapter is dedicated to explaining the use of phonopy as well as the necessary steps to obtain phonon properties and Grüneisen parameters. The last section of this chapter will then deal with the required steps to calculate phonon lifetimes.

Before the discussion on quantum mechanical simulation software starts, the source of the crystal structures shall be mentioned. Except for the structure of polyparaphenylene, all crystal structures were obtained from the Cambridge Structural Database[52]. For the materials biphenyl, fluroene, naphthalene, anthracene and pentacene the structures BIPHEN[53], FLUREN01[54], NAPHTA31[55], ANTCEN14[56] and PENCEN04[57] were used, respectively. Finally, the crystal structure for polyparaphenylene was taken from a paper by C. Ambrosch-Draxl et al.[58]

3.1. Quantum Mechanical Simulation Software

At the beginning of this thesis, the first-principles density functional theory (DFT) software package VASP was considered because of the superior accuracy. Phonons were obtained for fluorene and naphthalene. For polyparaphenylene, DFT proved to be too expensive from a computational point of view. The computational effort was too large to perform calculations on a large enough supercell to converge force constants sufficiently and, therefore, to obtain meaningful phonon properties. Consequently, a different simulation approach had to be considered and finally, the tight-binding based program DFTB+[59] was chosen, as it has shown reasonable accuracy compared to DFT at much lower computational cost.

3.1.1. VASP

VASP (ver. 5.4.1)[60–63] was used employing the projector augmented wave method[64] with the PBE functional[40]. To ensure proper results, the sampling density in the first Brillouin zone was converged to a difference in total energy of 1meV per atom. For fluorene and naphthalene Monkhorst-Pack[65] grids with 2x1x3 and 2x3x2 k-points were sufficient. The second quantity that needed convergence testing was the cutoff energy of the plane wave basis set. Total energy

calculations were performed with cutoff energies up to 1200eV and a threshold of 1meV in energy difference per atom was applied. The chosen cutoff energy was 800eV for both materials.

Although VASP offers the ability to relax lattice parameters and atom positions which is set by the INCAR-tag IBRION, the relaxation was performed using the GADGET tool (ver. 0.98_150717)[66]. This tool handles the geometry optimization while VASP is used for the electronic calculations. The use of internal coordinates instead of cartesian ones accelerates the process of relaxation considerably. For relaxation geometry, the allowed error in total energy was set to EDIFF = 1E-4 eV. To account for van der Waals interactions, the dispersion correction method of Tkatchenko and Scheffler (TS)[34] was used. According to the VASP manual, the precision tag PREC was set to *accurate* for the relaxation. Due to its suitability for organic molecules, Lindh's model hessian[67] in conjunction with the Broyden-Fletcher-Goldfrab-Shanno (BFGS)[68–71] optimization algorithm was used. As convergence criterium for forces, a threshold of 1meV/Å was chosen.

For calculation of force constants, single point calculations were carried out by VASP. For this purpose, the EDIFF-tag was reduced to 1E-8 eV.

3.1.2. DFTB+

DFTB+ (ver. 18.1)[43] was used with the Slater-Koster file set 3ob-3-1[59]. For all calculations, the self-consistent-charge (SCC) approach was used. Again, a preliminary convergence test concerning the sampling density in k-space was performed, with the breaking condition for the SCC cycles of 1e-5. This test resulted in Monkhorst-Pak[65] k-grids 4x3x4, 2x2x2, 2x1x3, 2x3x2, 2x3x2 and 2x2x1 for polyparaphenylene, biphenyl, fluorene, naphthalene, anthracene and pentacene, respectively. As a threshold, again 1meV in total energy difference was used.

Concerning van der Waals interactions, two different dispersion correction methods were used with DFTB+, however, not for all materials both approaches were tested. For fluorene and naphthalene, relaxation and force constants calculation were performed using an implementation of TS[72] and the D3-method by Grimme et al[35]. For the other materials, TS was discarded due to its computational effort because of slowly converging dispersion energies. Comparing computation times, D3 was faster than TS by a factor of 250 to 280 times for fluorene and naphthalene, respectively. As additional information, it shall be mentioned, that the TS-implementation was done in an unofficial release (r4465), and therefore, the large computational effort could be down to bad performance optimization. To use the implementation of the D3 dispersion correction, it is required to use the

DFTB3 Hamiltonian[73]. This improvement contains *"an improved Coulomb interaction between atomic partial charges"* and *"the complete third-order expansion of the DFT total energy"*[73]. For the use of DFTB3, the Hubbard derivatives for C = -0.1492 and H = -0.1857, and a damping factor $\zeta = 4.00$, which controls the damping of short-range interactions, have to be provided. As a program default, a Becke-Johnson damping function was used with the following parameters: $a_1 = 0.5719$, $a_2 = 3.6017$, $s_6 = 1.00$ and $s_8 = 0.5883$. All quantities are given in atomic units. This setup of DFTB3+D3 was used to obtain the results presented in this work.

Relaxations were performed using the implemented Conjugate Gradient method, applying a threshold of 5.1E-9 eV/Å (1E-10 Ha/Bohr) for the maximum force component and the Self-consistent-charge-tolerance was lowered to 1E-10 e (1.602E-29 C). For all materials except pentacene, relaxation of lattice parameters and atom positions was performed separately, because a combined relaxation of both quantities led to large a computational effort and questionable results at the same time. However, for pentacene, this mixed-mode relaxation showed the best result compared to the step-by-step approach, concerning the total energy and the residual forces.

The tight value for SCC-tolerance was kept for the calculation of force constant.

3.1.3. VASP vs. DFTB+

Now, to underline the suitability of DFTB+ for calculation of vibrational properties, phonon properties of fluorene and naphthalene obtained with VASP and DFTB+ will be compared in the following. Before that, the lattice parameters obtained for fluorene and naphthalene using the above-mentioned approaches are compared (Table 1). For both materials, the VASP+TS method

Table 1: Comparison of lattice parameters obtained for fluroene and naphthalene using VASP+TS, DFTB+TS and DFTB3+D3-BJ.

	Fluorene			**Naphthalene**		
	VASP+TS	DFTB+TS	DFTB3+D3	VASP+TS	DFTB+TS	DFTB3+D3
a / Å	8.223	7.985	7.911	8.052	7.791	7.500
b / Å	18.702	18.239	18.256	5.860	5.741	5.781
c / Å	5.524	5.432	5.426	8.616	8.416	8.409
α / °	90.00	90.00	90.00	90.00	90.00	90.00
β / °	90.00	90.00	90.00	123.89	123.97	124.64
γ / °	90.00	90.00	90.00	90.00	90.00	90.00

results in the largest lattice parameters, which in turn should lead to eigenmodes of lower frequency compared to the DFTB approaches. The first vibrational property to compare, are the phonon eigenvectors at the Γ point. For this reason, a python script by Tomas Kamencek first seeks for similar eigenmodes and then calculates the dot product of according phonon eigenvectors. For perfect overlap, the dot product can reach a maximum value of one. Figure 4 shows the overlap of eigenvectors for phonons of fluorene. In the frequency range up to 100cm^{-1}, all phonon eigenvectors are identical. At the full frequency range, phonon eigenvector overlap is still

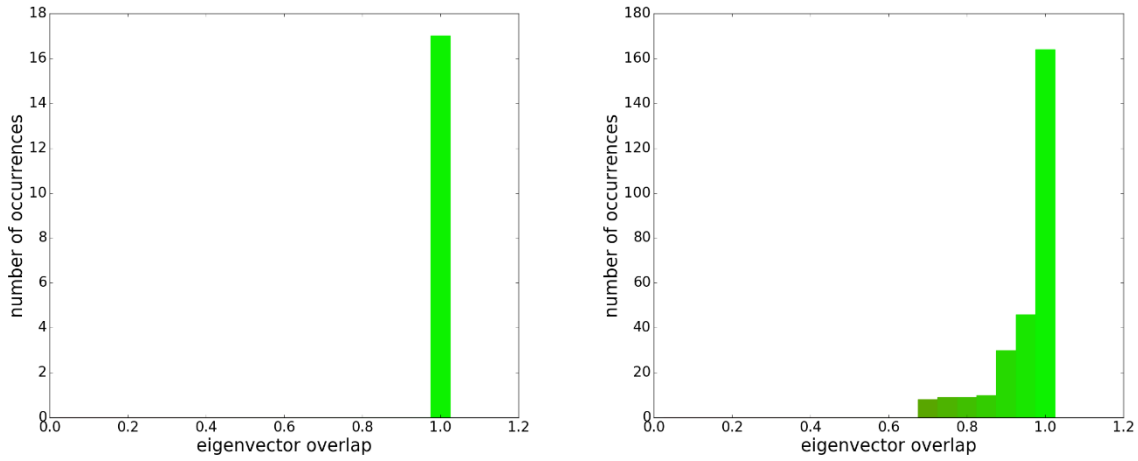

Figure 4: Comparison of phonon properties of fluorene at the Γ point obtained with VASP+TS and DFTB3+D3-BJ in terms of the dot product of eigenvectors. Phonon frequency ranges: 0-100cm^{-1} (left) and 0-3200cm^{-1} (right)

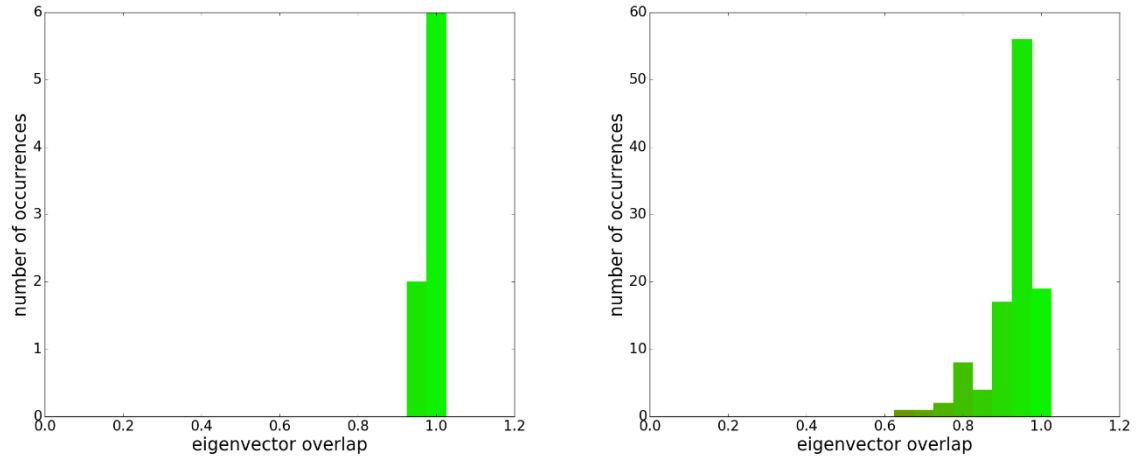

Figure 5: Comparison of phonon properties of naphthalene at the Γ point obtained with VASP+TS and DFTB3+D3-BJ in terms of the dot product of eigenvectors. Phonon frequency ranges: 0-100cm^{-1} (left) and 0-3200cm^{-1} (right)

acceptable, with more than half of the phonon modes showing identical eigenvectors. The same test was performed for the phonons of naphthalene, depicted in Figure 5. For this material, the obtained phonon eigenvectors are not as similar as for Fluorene. For the low frequency range up to 100cm^{-1}, only 2 out of 18 modes are not identical. At the full frequency range, the majority of phonons exhibit a dot product >0.94. In a second comparison, the phonon frequencies at the Γ point are shown as orange lines in the phonon density of states (DOS) (filled area). The compared simulation methods are VASP+TS, DFTB+TS and DFTB3+D3-BJ. The DOS was sampled within the first Brillouin zone on a 11x11x11 grid of q-points and a broadening of σ = 5cm^{-1} was used in all cases. For Fluorene (*Figure 6*), VASP+TS shows a pronounced first peak in the DOS compared to the other methods. In general, the agreement is better between VASP+TS and DFTB3+D3-BJ, than it is for DFTB+TS. Phonon frequencies obtained with DFTB+TS tend to be shifted towards higher frequencies. The situation for naphthalene (*Figure 7*) is similar, showing slight differences in the frequency range 0-100cm^{-1}. For this system, the agreement between both DFTB+ approaches is better, both phonon DOS are slightly shifted towards higher frequencies than for VASP+TS, which is a result of the slightly smaller unit cells obtained from DFTB+ (see Table 1).

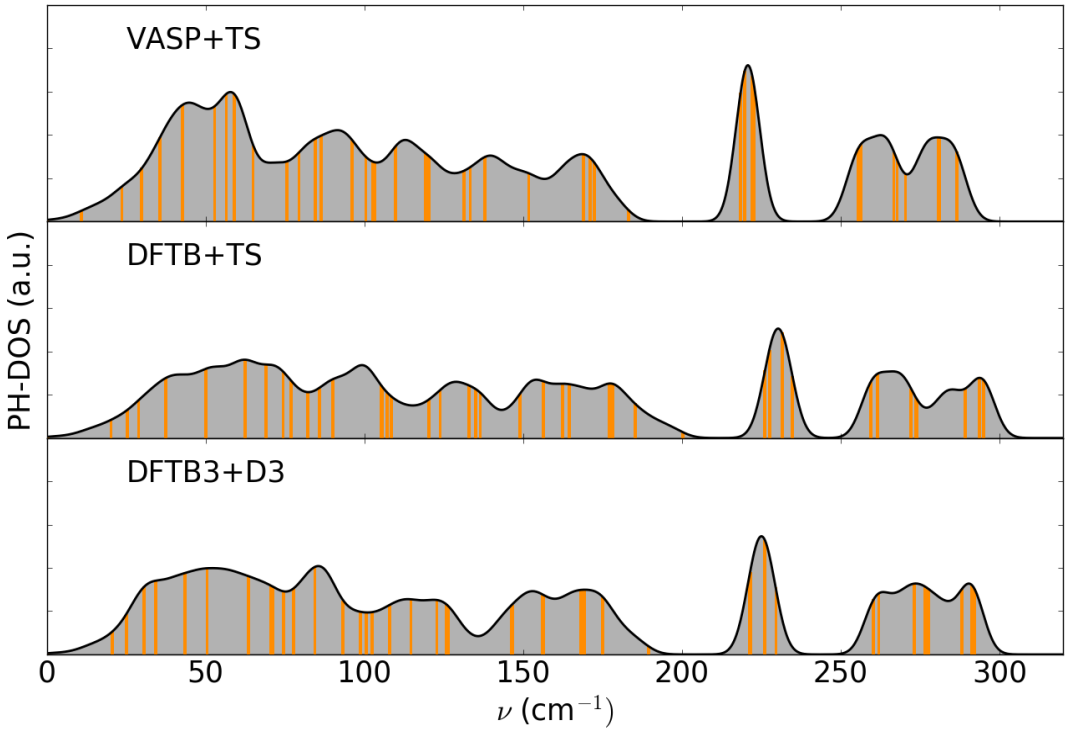

Figure 6: Comparison of phonon frequencies (orange lines) at the Γ point obtained for fluorene using VASP+TS, DFTB+TS and DFTB3+D3-BJ on the frequency range 0-300cm^{-1}

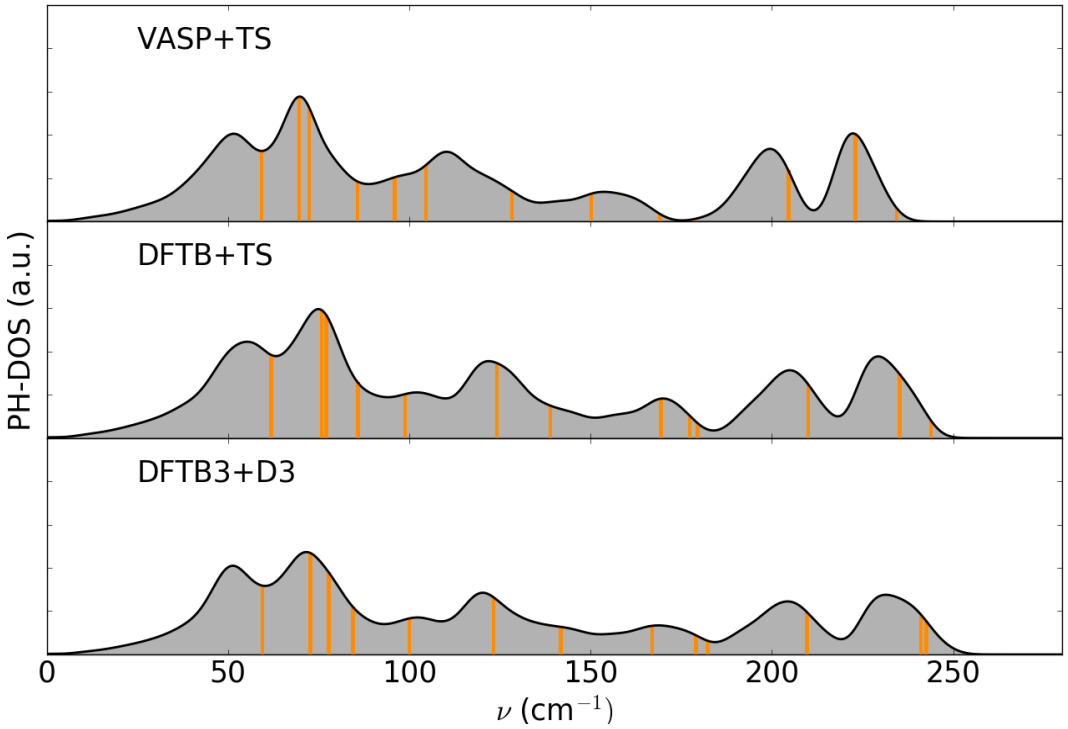

Figure 7: Comparison of phonon frequencies (orange lines) at the Γ point obtained for naphthalene using VASP+TS, DFTB+TS and DFTB3+D3-BJ on the frequency range 0-250cm^{-1}

Furthermore, the band structures for fluorene and naphthalene were compared. For the calculation of the band structures, 101 sampling points between each high symmetry points were considered. A comparison of the band structures for the two discussed materials obtained with VASP+TS and DFTB3+D3-BJ can be found in Appendix A.

3.2.Phonopy

For the calculation of phonons, the open source package phonopy (ver. 1.11.14-r1)[74] was used. Moreover, also the Grüneisen parameters were obtained with this program. Phonopy uses the finite differences method to obtain the derivatives of the potential energy with respect to the displacement of an atom according to section 2.3. The creation of supercells with one atom being displaced is done by phonopy via an interface to VASP. On the different displacement setups, single point calculations are performed to achieve the total energy and the forces acting on the not displaced atoms, which are extracted by phonopy to obtain the force constants. Phonon properties are finally calculated using a postprocessing step, after phonopy has created and diagonalized the dynamical matrix. As there is no interface to DFTB+, a script by Tomas Kamencek was used to convert the geometry file used by DFTB+ into a POSCAR file, used by VASP. After construction of

displacement setups, the VASP geometry file POSCAR was translated back to the geo.gen file required by DFTB+.

As mentioned in section 2.3, depending on the symmetry inherent to the present structure, the number of different displacement setups varies. The accuracy applied to find the symmetries of the structure can be manually adapted with the command option --tolerance, which is by default 1e-5Å. This setting had to be adjusted when using VASP/GADGET for relaxation, not so for the use of DFTB+. For naphthalene (VASP+TS), the default tolerance setting gave 216 displacements, a lower value of 1e-3Å equaled 54 different setups. To obtain converged force constants, it was found, that the k-grid values could be used as factors for the according supercells. An exception to this rule of thumb made pentacene, where a 4x3x2 supercell was required for converging force constants.

There are some important "seeting tags" to obtain physically meaningful results in phonopy. To enforce the sum rule for acoustic phonons, FC_SYMMETRY = .TRUE. is required. The group velocities, necessary for the calculation of the thermal conductivity are obtained by setting the GROUP_VELOCITY-tag. For this quantity, a nonsymmetric sampling mesh is required, which is imposed by MESH-SYMMETRY = .FALSE. Otherwise, one would not only need to weigh the properties according to their occurrence in the irreducible Brillouin zone, but also perform according symmetry operations.

3.3. Phonon Lifetimes

Phonon lifetimes were calculated in accordance with the lifetime model by Bjerg, discussed in section 2.4. Necessary ingredients to this model are a temperature scaling factor Θ, the average atomic mass in the unit cell M, the volume of the unit cell V, the speed of sound s and the mean squared Grüneisen parameter $\langle(\gamma^2)\rangle$ which are all present in equation (*2.21*). The temperature scaling factor was calculated according to equation (*2.22*) where the cutoff frequency ν_{cut} had to be chosen. In this work, the cutoff frequency was chosen to be the maximum frequency of any acoustic band. The average atomic mass and the unit cell volume could easily be extracted from the structural data. To obtain the speed of sound, group velocities were sampled on a dense, spherical mesh around Γ point. The velocity values were then averaged using a relation based in the Debye model:

$$s = \left(\frac{1}{3} \sum_{i=1}^{3} \frac{1}{s_i^3} \right)^{-1/3} \qquad (3.1)$$

To obtain the mode Grüneisen parameters according to (*2.17*) and (*2.18*), three dynamical matrixes corresponding to three different volumes are required. In the publication by Bjerg et al., the unit cell volume is modified and in a subsequent relaxation step, the lattice parameters are relaxed while keeping the modified unit cell volume constant. In contrast to that, in this work the unit cell's volume was contracted/expanded isotropically, i.e. the lattice parameters were multiplied by the factor 0.997/1.003. In the following relaxation step, only the atomic positions were allowed to change while the lattice parameters were kept constant. Subsequently, force constants were calculated for those modified cells to construct the required dynamical matrixes. The mode Grüneisen parameters were calculated using phonopy. The mean squared Grüneisen parameter was then calculated according to equation (*2.19*). Errors occurring from this slightly changed workflow compared to the originally published procedure were considered to be negligible. The ingredients to and the phonon lifetimes for the investigated materials are shown in Table 4.

4. Results

This section serves the purpose of presenting the results of this work that were obtained using the methods described in chapter 3. Prior to discussion of phonon properties, the obtained lattice parameters will be presented briefly because they are essential for phonon calculation. Like a music instrument, the size and shape do play an important role for the vibrations of the system, hence the crystal structures will be displayed as well. Harmonic phonon properties will be discussed subsequently, starting with the phonon density of states (Ph-DOS) to give an overview on the vibrational spectra of each material. The first harmonic ingredient to thermal conductivity is the phonon group velocity, which will be investigated with two different approaches. First, we will make use of the band structure, to access the phonon dispersion relation in a qualitative way and furthermore, to discuss anisotropy. In the next step, the group velocity is plotted against phonon frequency to allow for a quantitative comparison amongst the investigated materials. The second harmonic ingredient is the phonon mode heat capacity. To discuss the importance of the heat capacity for the calculation of thermal conductivity, the situation will be shown in an exemplary way for naphthalene. Before discussing then thermal conductivities, relevant quantities entering the phonon lifetime model and according phonon lifetimes are presented. The final subsection of this chapter will show the obtained thermal conductivities, their temperature dependence as well as their anisotropic behavior.

4.1. Lattice Parameters and Crystal Structures

The importance of lattice relaxation as preparation for phonon calculations has already been discussed in detail when the concept of lattice dynamics was introduced. Residual forces have to vanish to ensure that the system is at its equilibrium. Furthermore, changes of the crystal structure itself can have a big impact on phonon properties. A perfect example is the calculation of Grüneisen parameters. The unit cell is compressed and expanded by a small factor, however phonon properties like the frequency can vary tremendously (see Table 4). On the other hand, crystal structure itself depends on the applied quantum mechanical methodology and, particularly important for organic molecules, on the methods to account for dispersion forces.[51] For those reasons, this subsection is intended to present the lattice parameters obtained from DFTB3+D3-BJ, as those crystal structures are the basis of the following results. Illustrations of the crystal structures are presented alongside the respective phonon band structures in subsection 4.3.

*Table 2: Comparison of experimental and calculated lattice parameters. Where provided in the reference, experimental temperatures are given. ((1) unit cell was modified (b'=2*b), see text)*

	Polyparaphenylene		**Biphenyl**		**Fluorene**	
	Exp.	DFTB3+D3	Exp. @ 295K	DFTB3+D3	Exp. @ 295K	DFTB3+D3
a / Å	7.623	7.782	8.120	7.507	8.475	7.911
b / Å	5.523	10.745[(1)]	5.640	5.156	18.917	18.256
c / Å	8.701	8.672	9.470	9.195	5.717	5.426
α / °	89.750	90.00	90.00	90.01	90.00	90.00
β / °	107.626	106.98	95.40	90.52	90.00	90.00
γ / °	90.101	90.00	90.00	90.01	90.00	90.00

	Naphthalene		**Anthracene**		**Pentacene**	
	Exp. @ 5K	DFTB3+D3	Exp. @ 295K	DFTB3+D3	Exp. @ 90K	DFTB3+D3
a / Å	8.080	7.500	8.553	7.832	6.239	6.005
b / Å	5.933	5.781	6.016	5.750	7.636	7.091
c / Å	8.632	8.409	11.172	10.847	14.330	14.429
α / °	90.00	90.00	90.00	90.00	76.98	77.43
β / °	124.65	124.64	124.60	124.60	88.14	88.09
γ / °	90.00	90.00	90.00	90.00	84.42	84.41

Ab-initio codes produce results valid for a temperature of 0K. However, experiments to determine crystal structures are conducted at finite temperatures. Consequently, a comparison of calculated lattice parameters to experimental ones, as is shown in Table 2, is limited to a certain extent. Deviations are caused by the modeling approach and the thermal expansion, which was not investigated throughout this work. Although an in-depth comparison is denied by the aforementioned reasons, there are important aspects worth pointing out at this stage.

The investigation of polyparaphenylene was started using a unit cell with lattice parameters according to experiment, containing two molecules inside. Each of those molecules was set up from two phenylene rings covalently bonded at the para-position. Experimental[75,76] and computational[58] studies on polyphenylenes indicate an interring torsion angle of 18°. However, for relaxations using the gadget-tool and VASP in conjunction with the TS dispersion correction

method this result could never be obtained. Instead, a coplanar orientation of the phenylene rings was obtained (see Figure 8 (left)). To constrain the structure, the unit cell was doubled towards lattice parameter b and two additional molecules were added to obtain a different crystal symmetry. Relaxation of this modified structure finally resulted in a nonplanar configuration with an interring torsion angle of 15.4° (VASP+TS using the gadget tool) (see Figure 8 (right)). Although the problem of planar phenylene rings had been resolved, the increased cell size drastically increased the computational cost for subsequent phonon calculations. Consequently, the largest supercell affordable had the dimensions 2x2x2, which was not large enough for interactions to decay properly, resulting in imaginary phonons with negative frequency. In the course of switching the quantum mechanical methodology from VASP to DFTB+ the modified unit cell of polyparaphenylene was retained. Changing the methodology to DFTB+ finally allowed for calculation of a large enough supercell (4x3x4) to obtain meaningful phonon properties. The initial unit cell was again investigated applying DFTB3+D3. Relaxations were performed for cells with imposed orthorhombic and monoclinic symmetry, however, the total energy per atom and residual forces were larger than for the modified cell. Thus, no phonon calculation was performed for those structures.

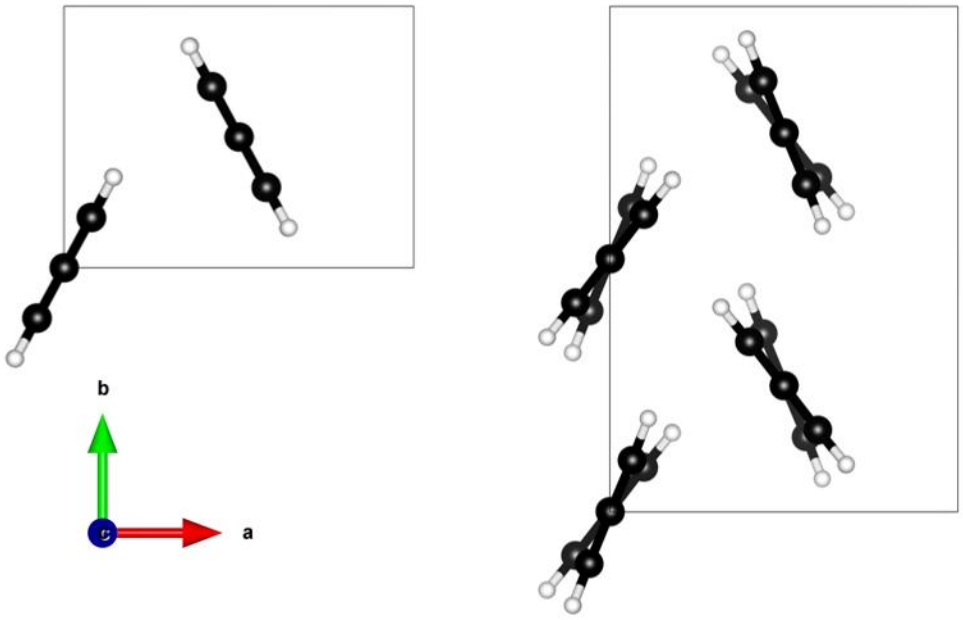

Figure 8: Crystal structure of polyparaphenylene after relaxation: phenylene rings are coplanar in the initial unit cell (left), phenylene rings are angled for interring torsion angle of 15.4° in the modified unit cell (right).

Concerning the obtained angles of the crystal structures, there is good agreement between experiment and simulation over all, except for biphenyl. For this material, the relaxation algorithm resulted in a much smaller angle $\beta = 90.52°$ instead of $\beta_{exp} = 95.4°$ (295K)[53]. For the other angles, the difference between measured and calculated values is smaller than 1%.

It has already been mentioned, that the correct description of vdW interactions is crucial to obtain correct crystal structures and subsequently to calculate correct vibrational properties for molecular crystals (see sec. 2.5.3). Due to the importance of vdW interactions, dispersion energies in eV per molecule and per atom are listed in Table 3.

Table 3: Dispersion energies of the investigated materials in eV per molcule and per atom.

Material	PPP	Biphenyl	Fluorene	Naphthalene	Anthracene	Pentacene
$\mathbf{E_{disp/molecule}}$ **/ eV**	1.899	2.103	2.073	1.692	2.335	3.710
$\mathbf{E_{disp/atom}}$ **/ eV**	0.095	0.096	0.090	0.094	0.097	0.103

As expected, the dispersion energy per molecule for acenes increases with increasing molecular size, i.e. increasing number of atoms in the molecule. The dispersion energy per atom also increases because the ratio of hydrogen atoms to carbon atoms decreases from 0.8 for naphthalene to 0.63 for pentacene. For biphenyl and polyparaphenylene the dispersion energies per atom are virtually the same differing by 1 meV. Fluorene exhibits the lowest dispersion energy per atom, which could be related to the methylene group denying a more densely packing, which would increase vdW interactions.

4.2. Phonon Density of States

One way to illustrate the vibrational properties of a system is by means of the phonon density of states. It displays the density of vibrational eigenstates of the system which can be occupied by phonons with respect to frequency. The peak heights relate to the number of vibrational eigenstates at a certain frequency. The phonon density of states was calculated on a grid of 11x11x11 q-points, which is sufficient in terms of convergence. Furthermore, the phonon density of states was normalized to the number of eigenmodes (3N, N … number of atoms) and a broadening of 1 and 5 cm^{-1} was applied (see figure caption). For all materials the phonon density of states in Figure 9 show vibrational states on a frequency range up to 1800 cm^{-1} (biphenyl ~ 1600 cm^{-1}) and a peak of high intensity at 3000 cm^{-1}. This peak is related to vibrations of the hydrogen atoms in which the bond between the hydrogen and carbon atoms is stretched. For the investigated materials, except

Fluorene, the hydrogen atoms are bonded to one carbon atom each, thus the strength of the bond is similar. Consequently, the vibrational eigenstates are in a very narrow frequency range which leads to the high intensity of this peak. For Fluorene, the phonon density of states shows a second, smaller peak at a slightly lower frequency (~2940 cm^{-1}) which is related to vibrations of the two hydrogen atoms of the methylene group. Those atoms are weaker bonded than the aforementioned hydrogen atoms, which relates to a lower vibrational frequency. For the studied acenes, this hydrogen-peak is increasing with increasing size, which is attributed to the increasing number of hydrogen atoms overall leading to more vibrational eigenstates of similar frequency. According to the narrow width of the hydrogen peak, those phonons are only weakly dispersed, or in other words, they are strongly localized at the molecule with vanishing group velocity. Therefore, those phonons have a negligible contribution to thermal transport. In Figure 10 the phonon density of states is displayed on a frequency range from 0-500 cm^{-1}.

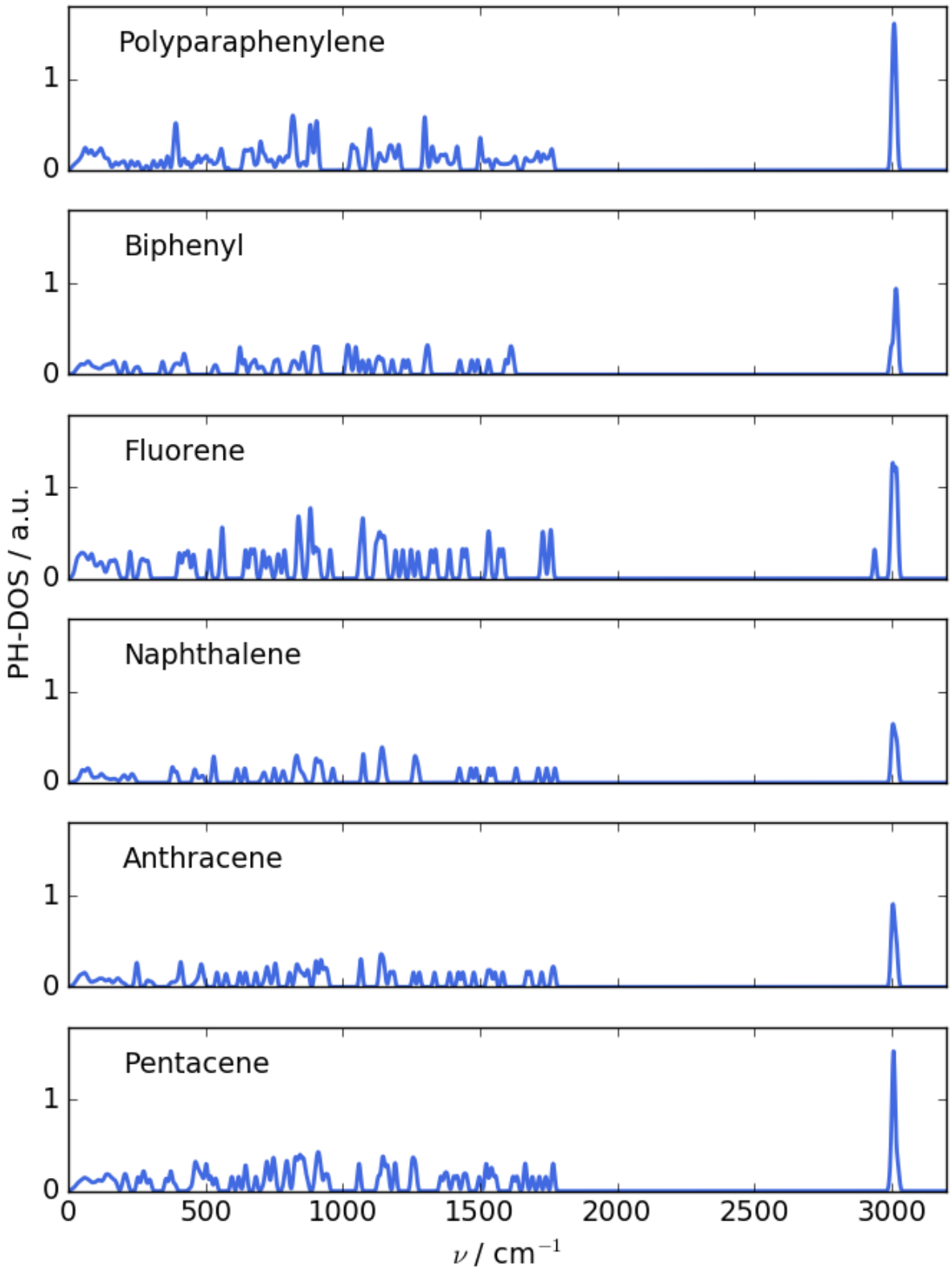

Figure 9: Phonon density of states (Ph-DOS) of the investigated materials on the full frequency range (σ=5cm^{-1})

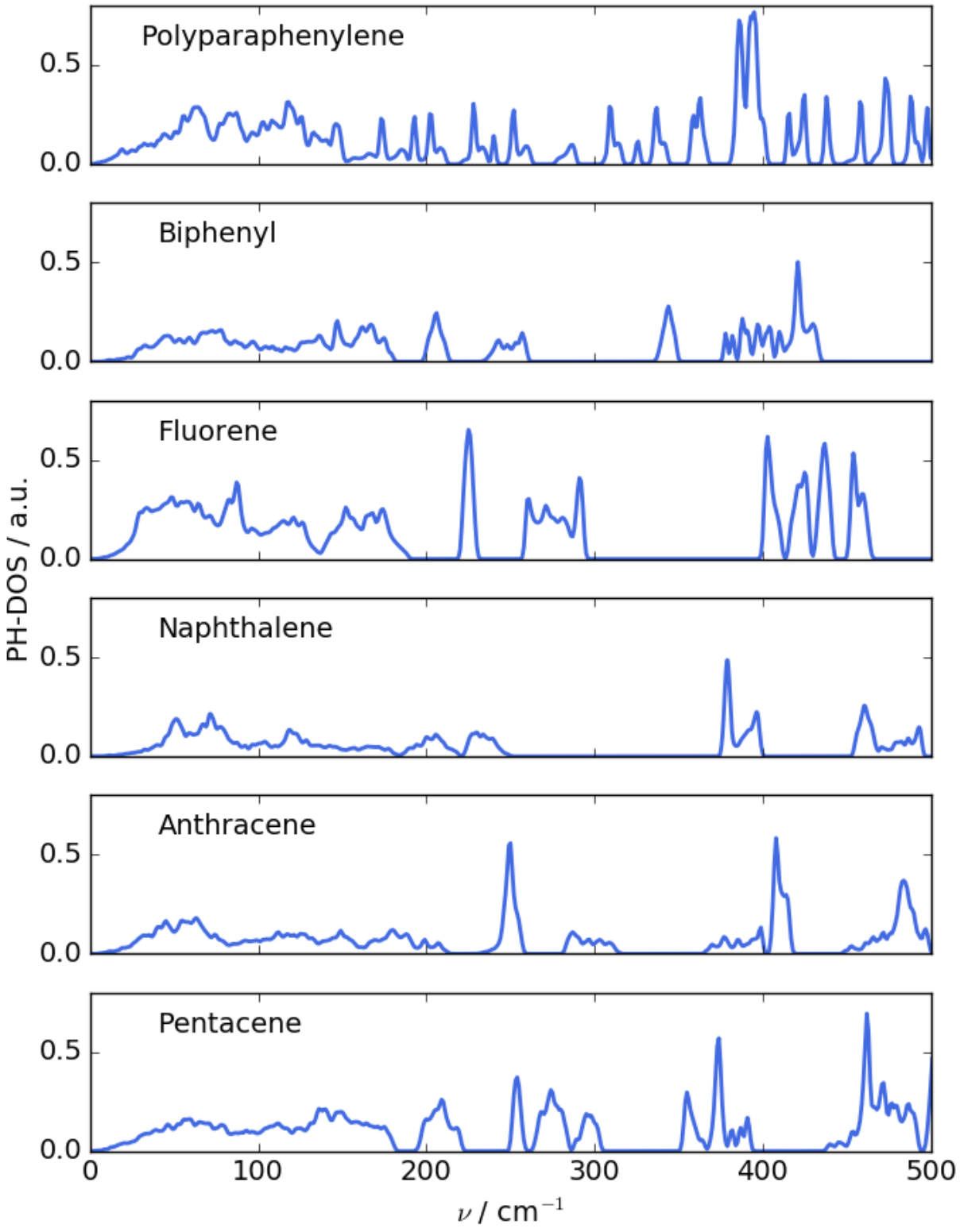

Figure 10: Phonon density of states (DOS) of the investigated materials on the frequency range 0-500cm^{-1} (σ=1cm^{-1})

4.3.Band Structures

The following subsection will be used, to discuss the phonon band structures of the investigated materials. The band structure shows the dispersion of phonon bands, or in other words, it relates the phonon frequency to the wavevector q. Since q has three cartesian components a four-dimensional plot would be necessary for representation. A more convenient illustration makes use of crystal symmetry. The phonon dispersion is obtained for wavevectors pointing along a path between high symmetry points of the first Brillouin zone. Therefore, the two-dimensional band structure allows the illustration of the phonon dispersion along different directions. This allows a qualitative investigation of the anisotropy of phonon band dispersion.

In the following, the phonon band structures for the investigated materials are shown and discussed. The according Brillouin zones are displayed to relate the high symmetry points of the band structure to actual directions in reciprocal space. Alongside, the crystal structures are presented to finally relate the band structure to directions in real space. The selected paths along high symmetry points are adapted from Setyawan and Curtarolo.[77] The plots of the Brillouin zones (are reprinted from Computational Materials Science, 49, Setyawan and Curtarolo, High-throughput band structure caclculations: Challenges and tools, 299-312, 2010, with permission from Elsevier.

Although eigenmodes in organic molecules can reach frequencies of up to around 3000 cm^{-1} the following band structures display the phonon dispersion relation for a lower frequency range. One reason for the importance of the low frequency region is the occupation of eigenmodes by thermal activation. Another argument to focus more on this low frequency region is group velocity. In general, optical phonons are less dispersed than acoustic ones, resulting in lower group velocities for the former ones and higher group velocities for the latter. Another important aspect is phonon scattering, which increases with phonon frequency. Therefore, it is less likely for high frequency phonons to contribute to thermal conduction at all, hence the upcoming discussion will focus on the frequency range from 0 to 300 cm^{-1}.

The last point to make before discussing the band structures is to mention the concept of external and internal modes as mentioned in the introduction. The forces present in an organic crystal are covalent bonds inside the molecules as well as dispersion forces between the non-polar molecules. Because of the strong forces within the molecule the frequencies of internal vibrations are higher than the frequencies of external modes. Generally, the number of eigenmodes is 3N, where N is the number of atoms in the unit cell. If one considers now a unit cell that contains m molecules

with n atoms per molecule, there are 3mn modes of which 6m are external and 3mn-6m are internal modes. In contrast to single atoms which only have three translational degrees of freedom, molecules have three rotational degrees of freedom additionally. For the materials polyparaphenylene and fluorene which contain 4 molecules in the unit cell, there are 24 external modes. The other materials all incorporate two molecules per unit cell equaling 12 external modes.

Polyparaphenylene

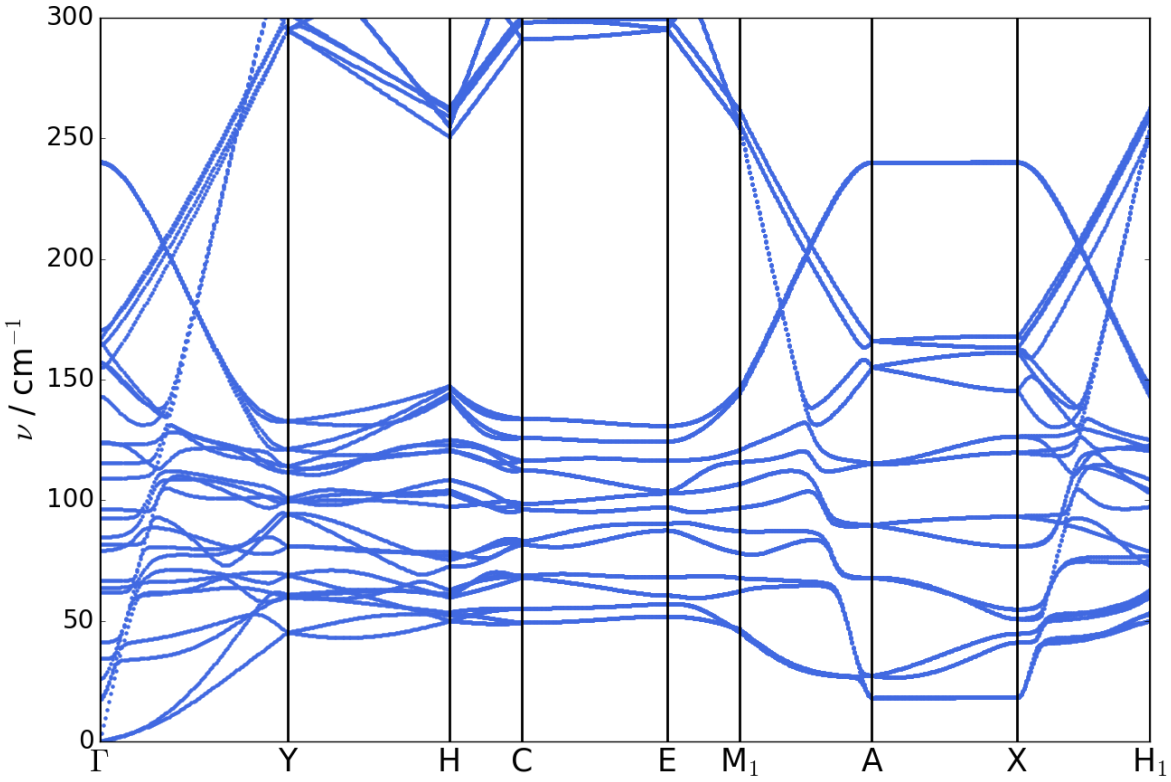

Figure 11: Band structure of polyparaphenylene with c-centered monoclinic crystal structure.

A remarkable aspect in the band structure of polyparaphenylene is the anisotropy of phonon dispersion. Phonon dispersion along paths Γ-Y, M_1-A and X-H_1 which are all parallel to b_3, is very strong. Furthermore, b_3 coincides with the direction of the covalently bonded polymer chains. Perpendicular to the polymer chain direction, Y-H, C-E and A-X, dispersion and therefore group velocity almost vanishes, resulting in localized phonons. For direction H-C and E-M_1, phonon dispersion is intermediate.

Another interesting aspect about PPP's band structure is the band gap of at least 100cm^{-1} that occurs along the path Y-H-C-E-M_1. This bandgap should limit three phonon processes because of energy

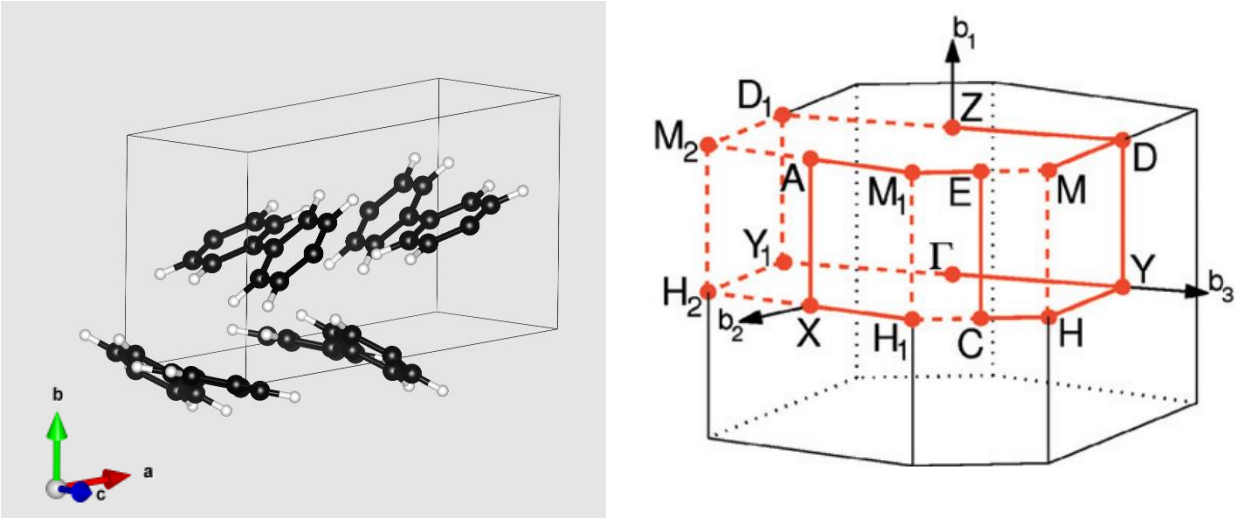

Figure 12: Crystal structure of polyparaphenylene[82] (left) and the according 1. Brillouin zone[77] (right). The molecular chain is parallel to c in real space, which corresponds to direction b_3 in reciprocal space.

conservation. Phonons of less than 150cm^{-1} cannot scatter into phonons at a frequency of 300cm^{-1}. However, the flat bands, particularly along the path C-E, should ease phonon scattering as the constraint of conservation of wavevectors is less important for flat, almost parallel bands.

Inspecting the path Γ-Y, at very low frequencies (even below 25cm^{-1}) optical phonons are present. Those optical phonons show a translational motion along the molecular chain, similar to longitudinal acoustic phonons, however, the center of mass doesn't change its location (in contrast to acoustic phonons). Due to the same symmetry of eigenmodes, those modes can hybridize. As a consequence of hybridization, avoided crossings occur. The stronger the coupling between two eigenmodes, the greater is the gap at the avoided crossing point. In the case of zero coupling phonon bands cross. Phonon hybridization can cause increased scattering, as has been shown by Wu Li et al[78]. Even slight hybridization of acoustic and optic phonons can decrease the lifetime of acoustic phonons a lot, hindering phonon transport.

One important value for the applied phonon lifetime model is the maximum acoustic phonon frequency. For polyparaphenylene this value was found to be 59.7 cm^{-1} close to the Y-point.

Biphenyl (base-centered orthorhombic)

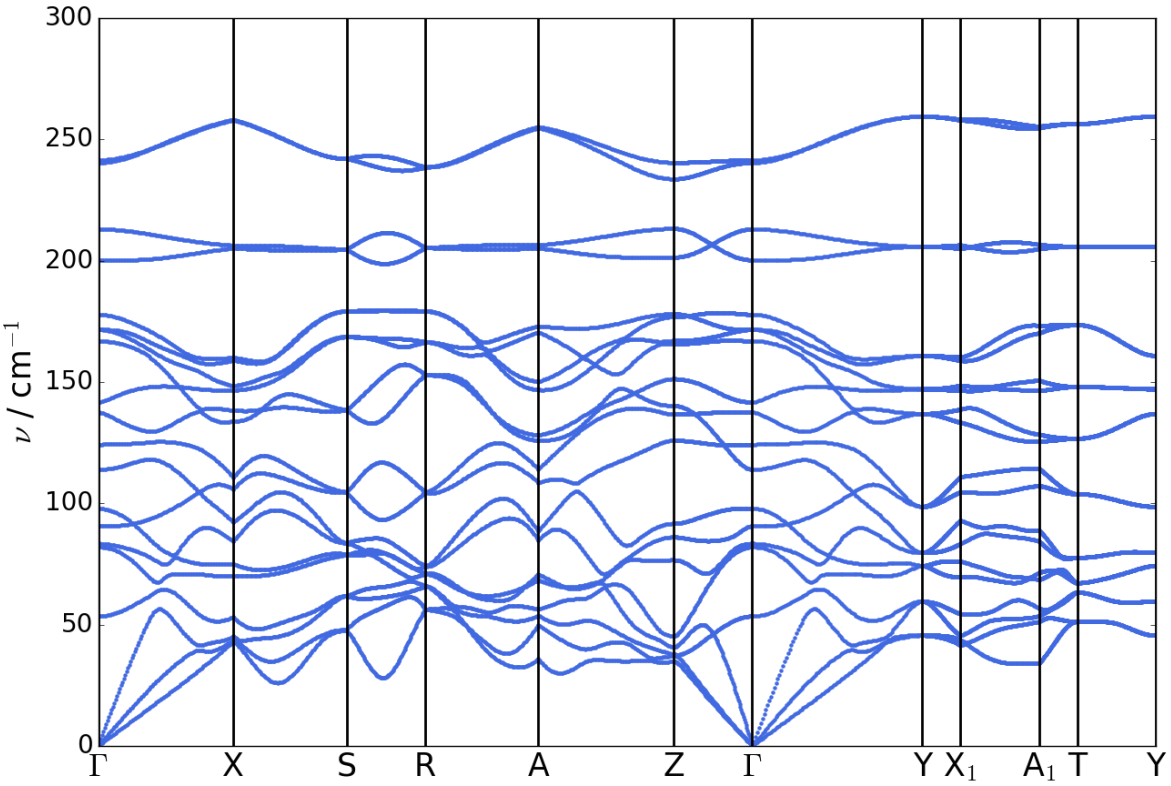

Figure 13: Band structure of biphenyl with base-centered orthorhombic crystal strcuture.

Tracing the longitudinal acoustic eigenmode (strongest dispersion of acoustic modes) along the path Γ-X (direction [110]), there is a beautiful example for phonon hybridization, which results in an avoided crossing and in return limits the maximum frequency of this branch. However, the trend of the eigenmode can be traced up to the Brillouin zone border. The same is true for the longitudinal acoustic mode along Γ-Y. Along the direction Γ-Z there no avoided crossings are present, the maximum acoustic frequency, however, is even lower compared to the other two cartesian directions. The maximum acoustic frequency is located close to the Y-point at 59.6cm^{-1}.

The dispersion of the bands is stronger for lower frequencies up to 175cm^{-1} compared to the localized phonons above. Many bands are degenerate at the high symmetry points, however they split up along the path between those points. This is particularly obvious for the path X-S-R-A. Between T-Y, no band splitting is present, and the bands are degenerate.

The four localized modes, two at 200cm^{-1} and the other two around 250cm^{-1} are eigenmodes corresponding to in-plane and an out-of-plane bending motion, respectively. Those modes are of

particular interest for structure-to-property relationships and will be discussed later on (cf. section 5.1).

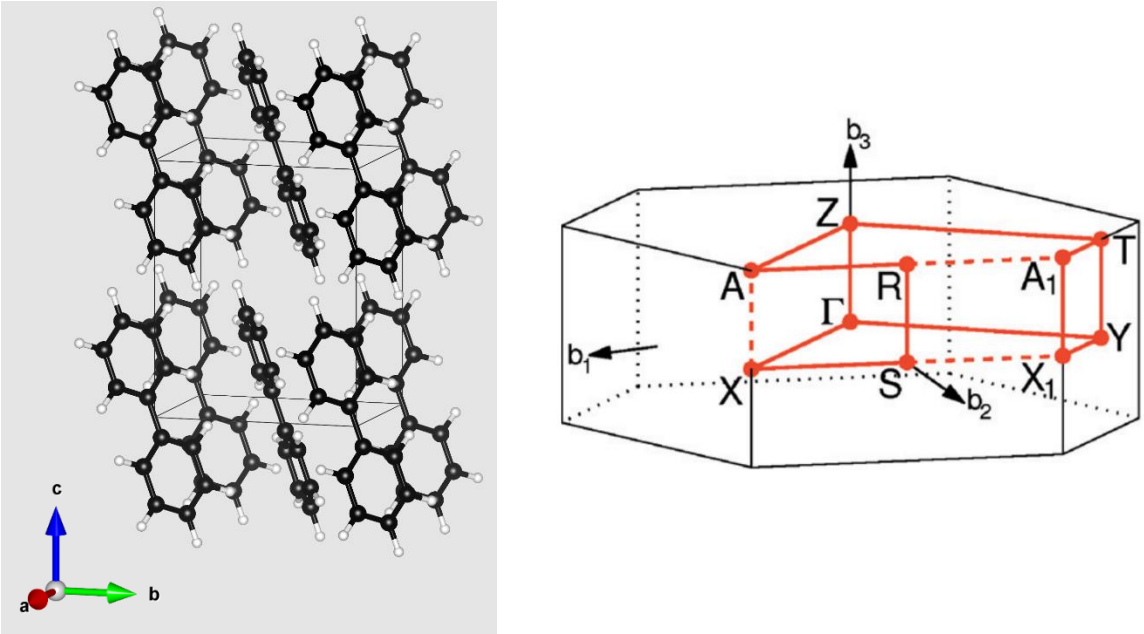

Figure 14: Crystal structure of biphenyl[82] (left) and according 1. Brillouin zone[77] (right). The molecules are slightly angled with respect to direction c which corresponds to b_3 in reciprocal space.

Fluorene

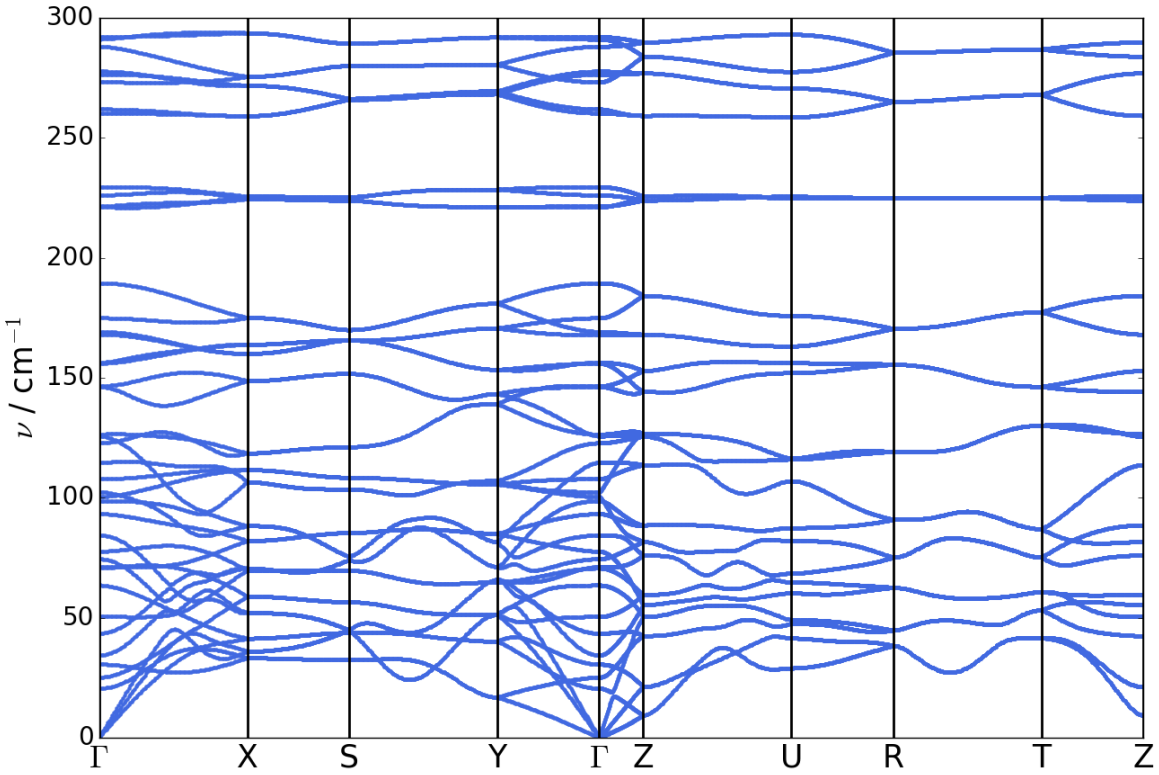

Figure 15: Band structure of Fluorene with orthorhombic crystal strcuture.

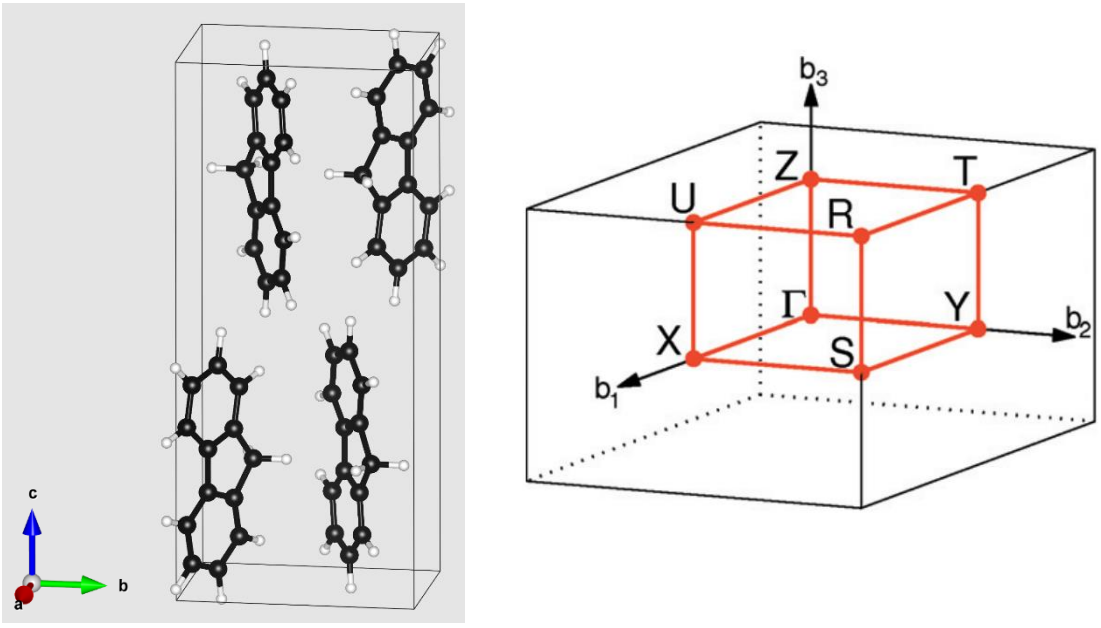

Figure 16: Crystal structure of fluorene (left) and the according 1. Brillouin zone (right). The molecules are oriented towards the c direction, which corresponds to the reciprocal direction b_3.

With four molecules per unit cell, the band structure of fluorene exhibits 24 external modes. They cover a frequency range up to roughly 125cm^{-1} at the Γ point with the lowest optical band starting below 25cm^{-1} at Γ. Avoided crossings play a role again, especially on the paths Γ-Y (direction b) and Γ-Z (direction c). The maximum acoustic frequency was found to be at 50cm^{-1} located close to the Y-point. Except for paths Γ-X, Γ-Y and Γ-Z, bands are comparably weak dispersed. Many of the bands are degenerate at high symmetry points as well as on the path between those points. The very flat band at around 225cm^{-1} characterizes in-plane bending modes, the bands just below 300cm^{-1}, show the dispersion of eigenmodes with an out-of-plane bending motion.

Naphthalene

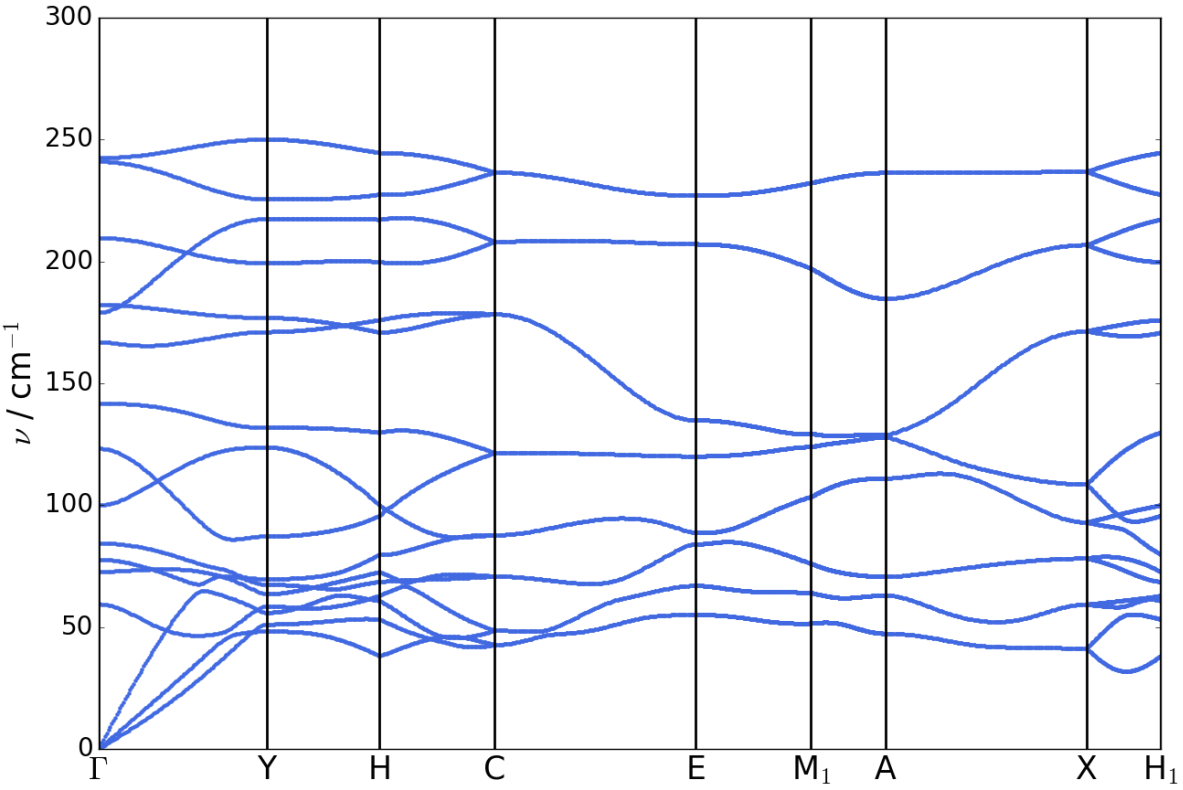

Figure 17: Band structure of naphthalene with c-centered monoclinic crystal structure.

The unit cell of naphthalene hosts two molecules and therefore the first 12 modes are considered external vibrations and range up to around 180cm^{-1}, except for the high symmetry points E, M_1 and A, where the frequency drops below 150cm^{-1}. Dispersion of bands is low for most parts of the band structure, only path Γ – Y (direction normal to plane a-b, normal to molecular layer) shows considerable dispersion. Hybridization of the longitudinal acoustic band and a low frequency

optical phonon cause again an avoided crossing, limiting the maximum frequency of the acoustic band. The maximum acoustic frequency was found to be 70.7cm^{-1} close to the Z-point, which is not displayed in the band structure. An interesting feature of the band structure is the occurrence of degenerate bands along the path C-E-M1-A-X. All those 8 bands present are twofold degenerate and show no band splitting, which means, that those eigenmodes possess the same energy.

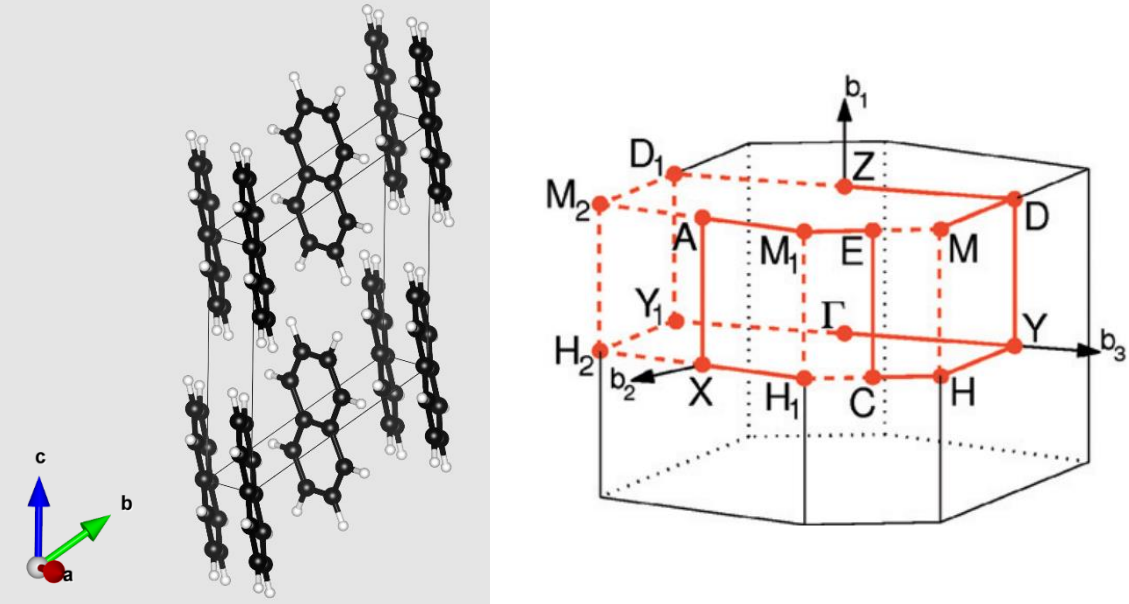

Figure 18: Crystal structure of naphthalene[82] *(left) and the according 1. Brillouin zone*[77] *(right). The molecules are parallel to c in real space, which corresponds to direction b_3 in reciprocal space.*

Anthracene

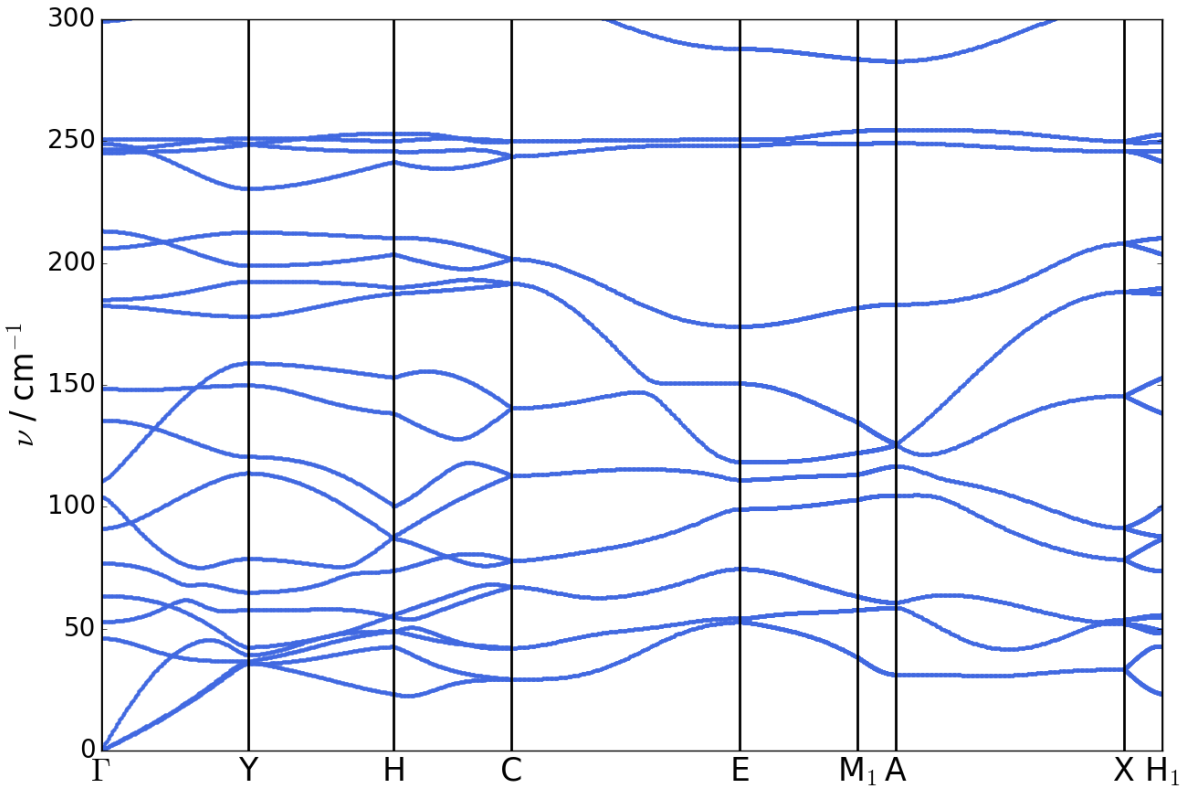

Figure 19: Band structure of anthracene with c-centered monoclinic crystal structure.

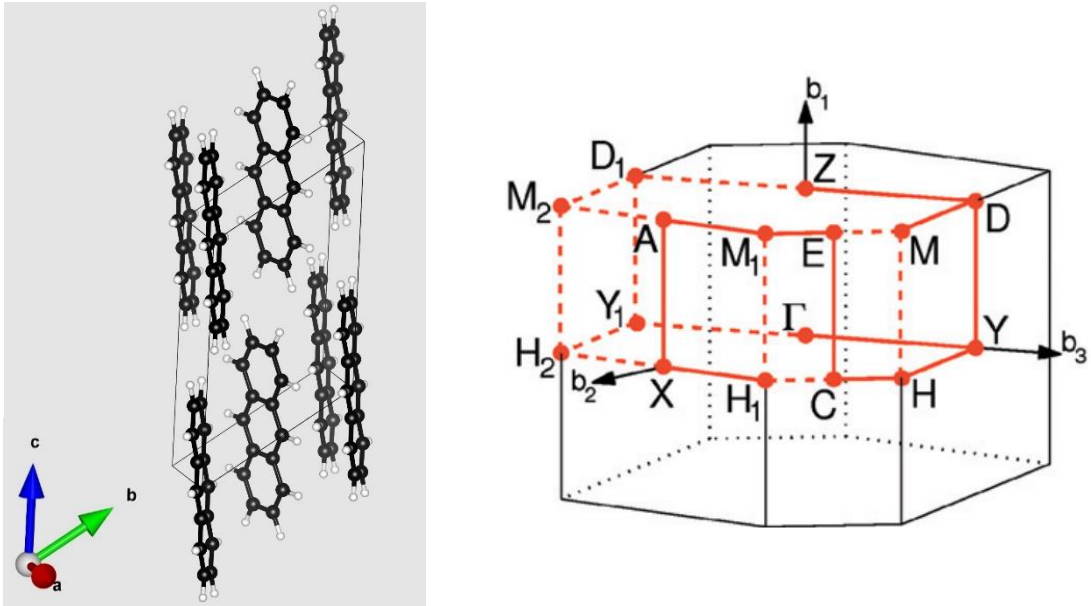

Figure 20: Crystal structure of anthracene[82] (left) and the according 1. Brillouin zone[77] (right). The molecules are parallel to c in real space, which corresponds to direction b_3 in reciprocal space.

The band structure of anthracene is very similar to naphthalene's. The external vibrations reach up to around 150cm^{-1}, lower than for naphthalene. Also, the first optical band at Γ is located at a lower frequency. Again, along the path C-E-M1-A-X, bands are twofold degenerate without any band splitting. The maximum frequency of an acoustic phonon was found to be 63.0cm^{-1} at the D point.

Pentacene

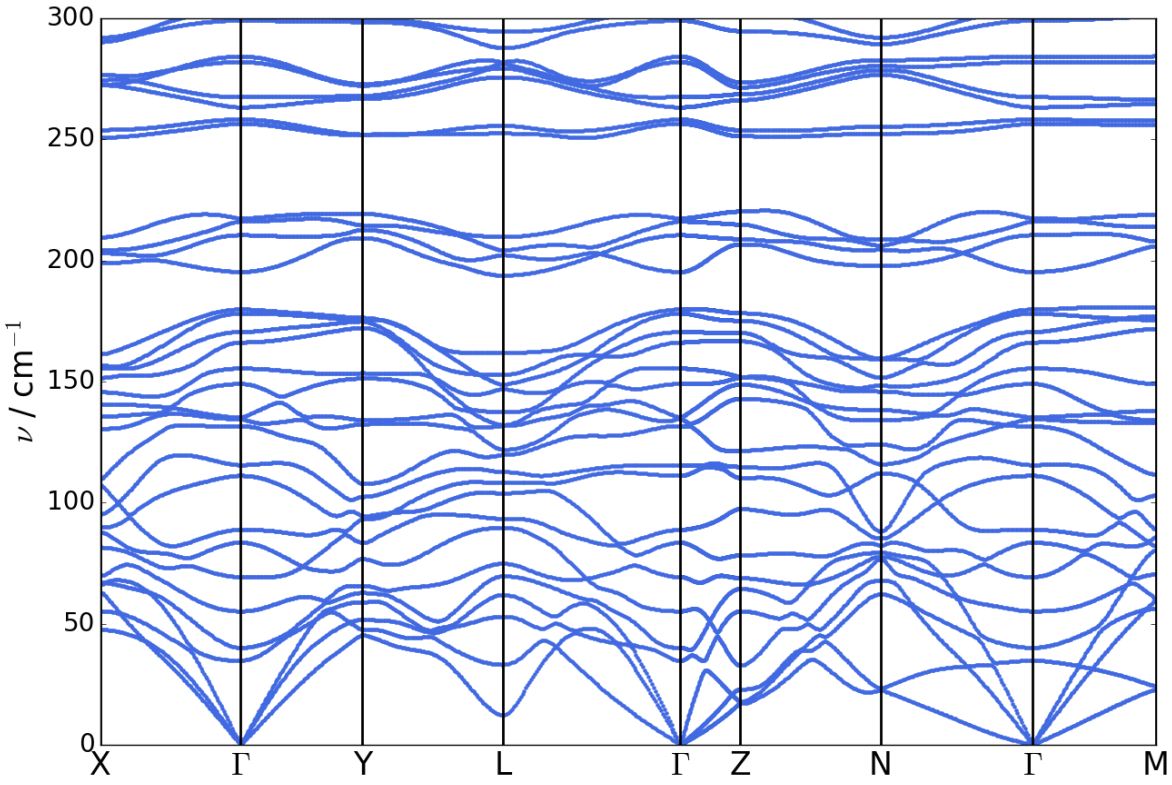

Figure 21: Band structure of pentacene with triclinic crystal structure.

In pentacene's band structure, a lot more eigenmodes are present compared to naphthalene and anthracene which is related to the large number of atoms, 72, in the unit cell. Following the trend from naphthalene and anthracene of decreasing maximum external vibrations frequency, this material's external vibrations range up to around 130 cm^{-1}. Avoided crossings are again present in the low frequency region between acoustic and optical eigenmodes. Along direction Γ- X (direction a), avoided crossings between the three acoustic and first two optical modes are present. The longitudinal acoustic mode is affected by two avoided crossings resulting in two kinks in its dispersion. Towards point Y, the second and the third acoustic mode avoid a crossing, close to the border of the Brillouin zone. The three lowest lying optical modes are interfering with the transversal acoustic mode, limiting its dispersion and maximum frequency. An interesting feature

of this band structure is the very low frequency (12.38 cm^{-1}) present at point L, corresponding to an energy of 1.5 meV. At the q-point (0.35, 0.35, 0) the two transvers acoustic modes cross, whereas crossings between the transvers and longitudinal modes are avoided. The strongest hybridization of eigenmodes, concerning the width of the gap at the crossing point occurs along the path Γ- Z (direction c). Close to Γ, the first two optical modes are avoiding a crossing, and thereby swap their dispersions. Increasing the distance from the Γ-point, the lower lying optical mode then interacts with the longitudinal acoustic mode limiting the maximum frequency drastically. After this avoided crossing, it looks like the optical mode is continuing the dispersion of the acoustic mode it hybridized with. For directions Γ – N and Γ – M, the band structure looks very similar concerning the low frequency region up to around 80 cm^{-1}. Again, the lowest lying optical mode is interfering with the strongest dispersed acoustic bands and in succession, those bands are then interfering with the intermediate dispersed acoustic bands. After all, the maximum frequency of the acoustic modes in pentacene is again limited due to the interference with low lying optical bands. The maximum acoustic frequency was found to be 62.9 cm^{-1} at the X-point.

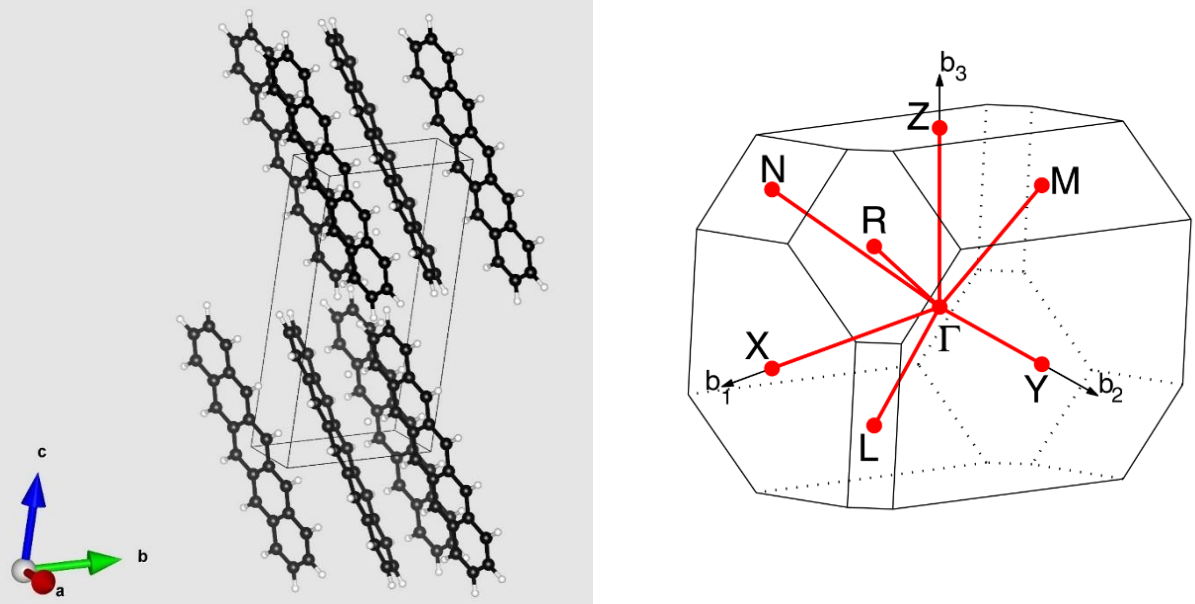

Figure 22: Crystal structure of pentacene[82] (left) and the according 1. Brillouin zone[77] (right). The molecules are tilted within the layers, which are stacked in direction c, corresponding to direction b_3 in reciprocal space.

4.4. Group Velocity

As outlined in the theory part, the group velocity of phonons is one harmonic ingredients to thermal conductivity and furthermore, it enters calculation as a squared entity. In the previous section, the phonon band structures were used to discuss the directional dependence in the phonon dispersion, which relates directly to the group velocities, in a qualitative way. However, to compare the group velocities amongst the investigated materials, quantitative values are required. Therefore, the effective group velocities are plotted against frequency in Figure 23.

Group velocities were calculated for all 3N phonons at frequency ν on a mesh of q-points within first Brillouin zone. For the materials biphenyl, naphthalene, anthracene and pentacene, the group velocity was obtained on q-grids of the size 33x33x33. Due to the large number of phonon modes in polyparaphenylene (240) and fluorene (276), less dense q-grids of the size 15x15x15 were taken. The effective group velocity was obtained from the three cartesian components. Please note, that for the speed of sound a different formalism was used to add the cartesian components (cf. equ. (*3.1*)). For this reason, the displayed group velocities are not meant to be compared to the speed of sound.

It would be favorable to plot the group velocities for each phonon band separately, which requires the identification of phonon bands at each q-point. Phonopy can handle this identification by consideration of the phonon eigenvectors. Unfortunately, this procedure is available only for calculation of the phonon band structure along paths in reciprocal space. In the mesh-sampling mode, this procedure is not provided, thus, phonons are sorted according to their frequency. Moreover, to obtain a reliable phonon band identification a dense sampling grid is recommended, which is computationally unfeasible. Consequently, the group velocities could neither be assigned to certain bands, thus in Figure 23 group velocities of all bands are plotted in dependence of the phonon frequency. Group velocities are plotted on the frequency range between 0 and 2000 cm^{-1} because of the absence of important features at higher frequencies. Between around 1750 and 3000 cm^{-1} there are no phonon modes at all and the already mentioned hydrogen bond-stretching modes at around 3000 cm^{-1} are strongly localized, thus their contribution to thermal transport can be neglected. As unit for the group velocities THzÅ was used which is the default unit of phonopy. This unit might appear cumbersome; however, it eases the calculation of the mean free path for phonon lifetimes given in ps. Expressed in m/s, 1 THzÅ equals 100 m/s.

At a glance, polyparaphenylene clearly exhibits the highest group velocities followed by pentacene which shows group velocities up to 100 THzÅ. Maximum group velocity for both biphenyl and fluorene is around 60 THzÅ, naphthalene's slightly exceeds 50 THzÅ and anthracene shows the lowest maximum group velocity of around 40 THzÅ. Common to all systems, group velocities are highest in the frequency region 0-200 cm^{-1}. For naphthalene and anthracene this frequency region reaches up to around 250 cm^{-1}. Compared to all other systems, the group velocities of polyparaphenylene are not vanishing even for high frequencies, except for a small frequency region around 1000 cm^{-1}. In the case of biphenyl and fluorene, there are comparably low group velocities at elevated frequencies. The three acenes have a group velocity feature in common just below 500 cm^{-1}. Anthracene and pentacene exhibit a very similar behavior for the frequency region from 200 to 1000 cm^{-1}. To sum this up, except for polyparaphenylene, the distribution of group velocities with respect to frequency shows, that the main contribution to thermal conductivity will arise from low frequency phonons which show comparably high group velocities. For polyparaphenylene, the frequency region of contribution to thermal transport could potentially reach above 1000 cm^{-1}.

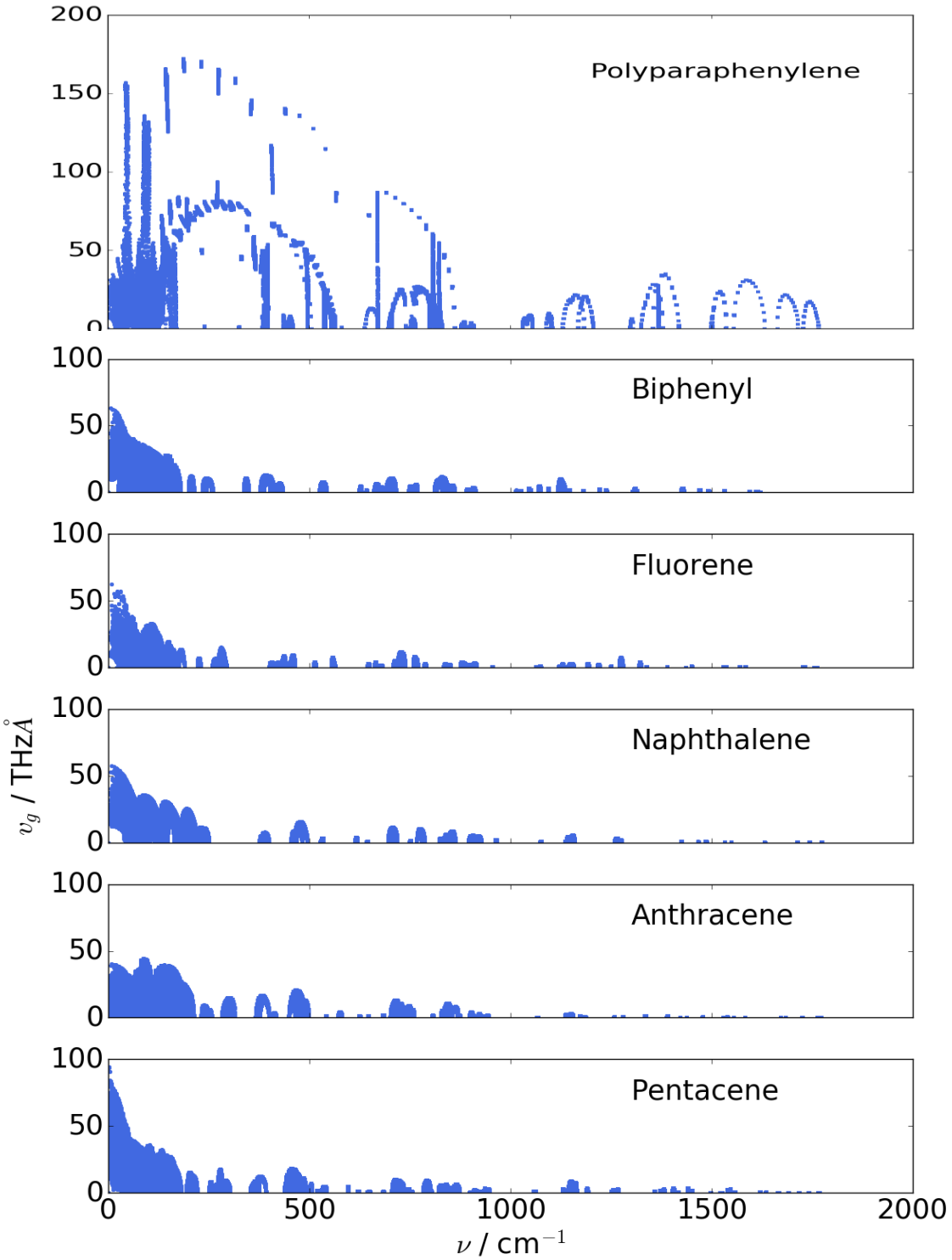

Figure 23: Effective group velocities sampled within the first Brillouin zone, plotted against phonon frequency. Please notice the different scaling of the y-axis for polyparaphenylene.

4.5.Heat Capacity

The second harmonic ingredient to be discussed is the phonon heat capacity. This is actually the only harmonic ingredient dependent on temperature. In chapter 2, the (cf. equ. (*2.8*)) phonon mode heat capacity was shown to be the first derivative of the Bose-Einstein distribution with respect to temperature. The function can be seen in Figure 2 for different temperatures. Its shape looks very much like the frequency response function of a lowpass. Basically, it also behaves like a lowpass filter; phonons up to a certain frequency or energy, dependent on temperature, can contribute to thermal transport. For high frequency phonons, the heat capacity vanishes. Hence, they cannot contribute to thermal transport. In Figure 24 the phonon heat capacity function at 300 K is plotted (red) as well as naphthalene's DOS multiplied with the heat capacity function. The full width at half maximum (FWHM) for this temperature is around 620 cm^{-1}. Therefore, considering the discussion on group velocities above, the heat capacity function is not the limiting factor for phonon mode contribution, unless very low temperatures are considered.

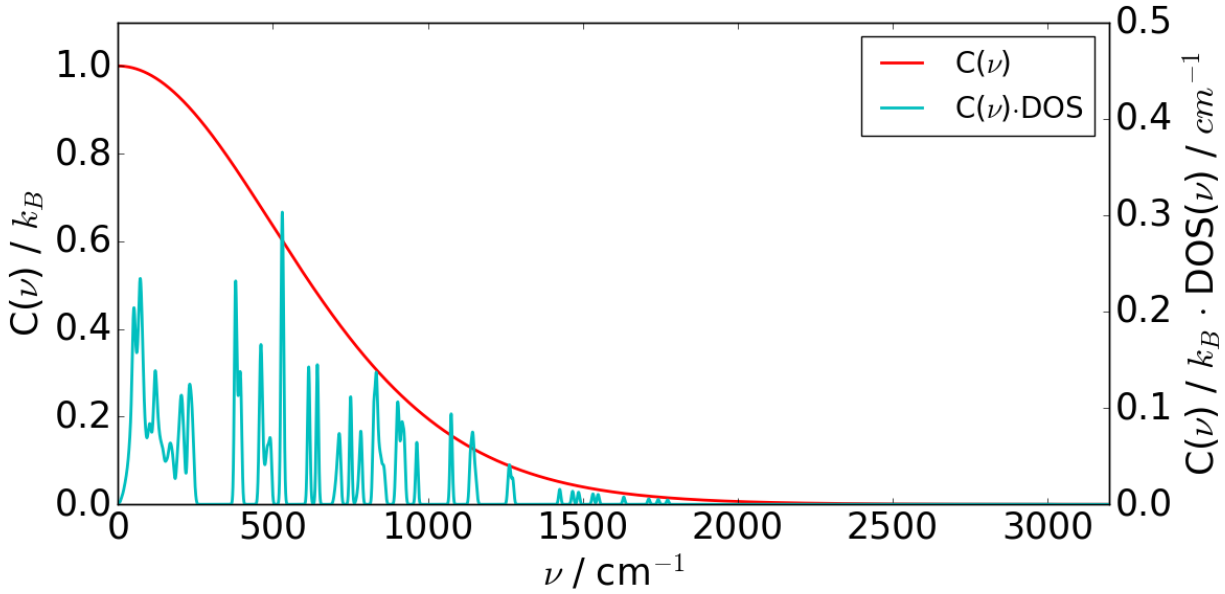

Figure 24: Phonon DOS of naphthalene multiplied by the phonon mode heat capacity function

4.6.Phonon Lifetime Model

Now that the harmonic ingredients are discussed the last missing quantity to calculate thermal conductivities is the phonon lifetime. The phonon lifetimes are obtained from an empirical model, according to section 2.4 and 3.3. This has shown reasonable results for a wide variety of, however, inorganic materials. The core idea of the applied model is to correlate the phonon lifetimes to the Grüneisen parameter (cf. equ. (*2.17*)). To be more precise, the mean squared Grüneisen parameter

(MSGP) is used, calculated according to equation (*2.19*) in order to avoid canceling of Grüneisen values of opposing sign. Other quantities entering the phonon lifetime model are the temperature scaling factor Θ, which depends on the cutoff frequency ν_{cut} (cf. equ.(*2.22*)), the unit cell volume, the average mass, and the speed of sound s. Except for the average mass and the unit cell volume all quantities entering the lifetime model are displayed in Table 4.

Table 4: Input quantities to the used phonon lifetime model and the resulting lifetime factor $\tau\omega^2$ for a temperature of 300K.

	PPP	**Biphenyl**	**Fluorene**	**Naphthalene**	**Anthracene**	**Pentacene**
MSGP / a.u.	3.853	6.048	4.119	5.088	4.436	3.899
ν_{cut} / cm^{-1}	59.71	59.71	50.03	70.72	65.71	62.93
Θ* / K	75.42	73.51	60.75	88.578	79.349	76.8775
s / ms^{-1}	3830.1	3451.1	3238.5	2934.5	3007.6	4608.2
$\tau\omega^2$ / 10^{12} s^{-1}	33.841	13.272	16.801	18.977	20.619	40.421

The MSGPs for tested materials are ranging from 3.853 for PPP up to 6.048 for biphenyl. A higher value indicates more internal anharmonicity which results in shorter phonon lifetimes. Concerning this quantity, there is a trend obvious for the modelled acenes. With increasing size of the molecule, the MSGP decreases, meaning less internal anharmonicity for pentacene compared to naphthalene. This could be related to the decreasing number of interfaces between the densely packed layers with increasing length of the molecules. The same trend is apparent for cutoff frequency and temperature scaling factor whereas speed of sound increases drastically. Considering the strong dispersion in the band structure of polyparaphenylene, one could conclude that in this material the speed of sound should be the highest. However, the speed of sound is obtained as an average of all three acoustic bands (cf. equ. (*3.1*)). Although polyparaphenylene's longitudinal acoustic eigenmode has a group velocity of around 14,000 m/s close to the Γ point, the transversal modes (2966 and 4077 m/s) lower the average a lot. This can be related to the strong covalent bonds along the polymer chain and the much weaker dispersion interactions acting perpendicular to it. In the case of pentacene, all three branches show group velocities exceeding 4300 m/s.

The last quantity in Table 4, $\tau \cdot \omega^2$, can be obtained from rearranging equation (*2.20*). It is used to calculate the phonon lifetime for a certain frequency. Figure 25 illustrates the phonon lifetimes over a frequency range up to 100 cm^{-1}, where they have already decreased to a magnitude of 10^{-3} ps.

To set the phonon lifetime values into perspective, given the group velocities are on the order of 10^1 THzÅ a mean free path on the order of the lattice parameters requires a minimum lifetime on the order of 10^{-1} ps. According to the graphs in Figure 25 these considerations narrow the frequency range for contribution to thermal transport to around 20 cm^{-1}. The fact that for vanishing phonon frequencies the phonon lifetimes are diverging is canceled by vanishing group velocities at the Γ point.

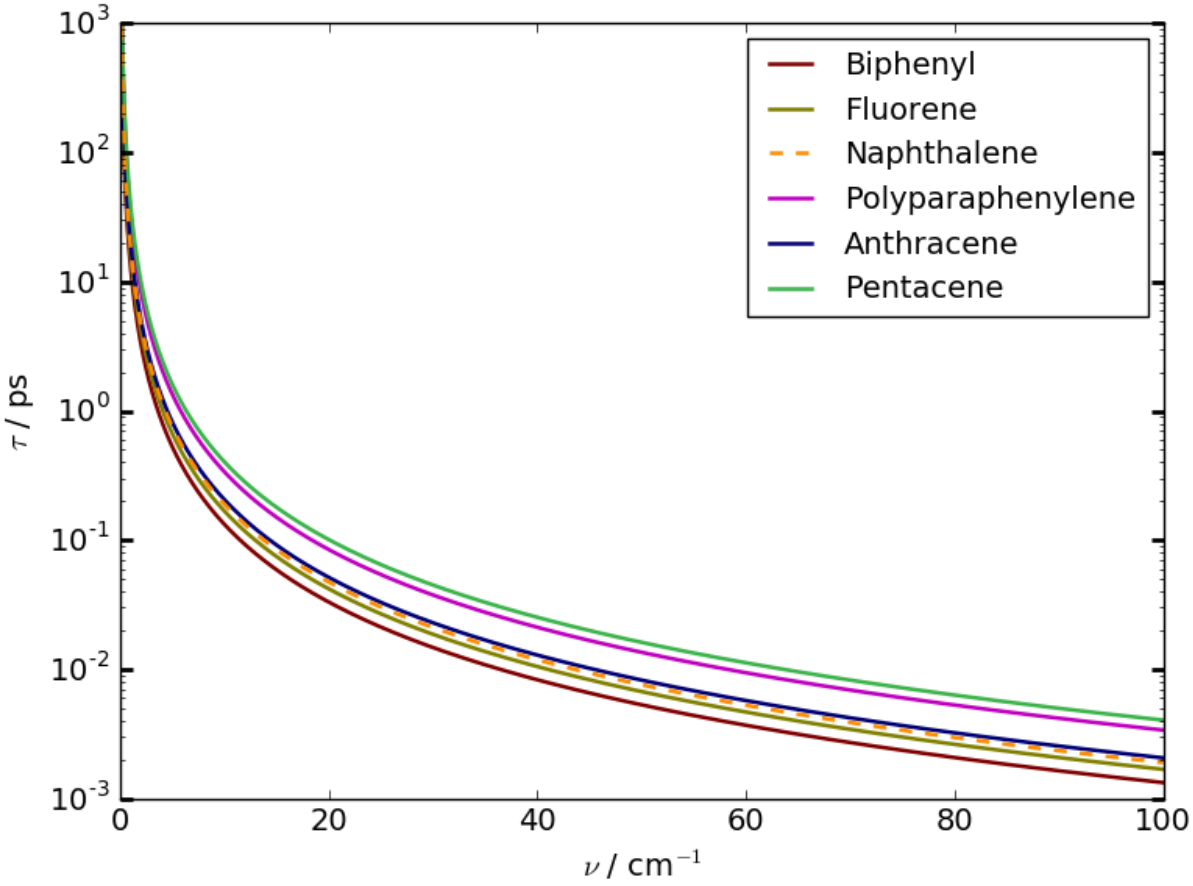

Figure 25: Phonon lifetimes in ps at 300K plotted versus frequency.

4.7. Thermal Conductivity

So far, all ingredients to calculate thermal conductivity have been discussed. The harmonic ingredients, heat capacity and group velocity, and the phonon lifetime as anharmonic contribution were shown.

The contribution of phonons to thermal conductivity with respect to frequency is limited by the heat capacity function to around 600cm^{-1} at room temperature. Except for polyparaphenylene, the band structures show a reasonable phonon dispersion not for the entire frequency range but rather

for lower frequencies. The group velocity plots show the same trend of comparably high group velocities present up to around 200 to 250 cm^{-1}, apart from polyparaphenylene. However, the phonon lifetimes restrict the contribution to thermal conductivity to very low frequencies. The contribution of each individual phonon mode to thermal conductivity is plotted as the green graph in Figure 26. It clearly shows the dominance of phonon lifetimes, as the contribution to thermal conductivity is limited to phonons of frequency below $100cm^{-1}$ apart from polyparaphenylene showing contribution of modes at around 150-200 cm^{-1} and pentacene, where phonons only up to around $50cm^{-1}$ contribute. To obtain the contribution to thermal conductivity of all phonons at a certain frequency the mode dependent contribution is multiplied with the phonon density of states (Figure 26 blue graph).

Comparing the frequency range given in Figure 26 to the band structures one can conclude that the contribution to thermal conductivity mainly arises from acoustic eigenmodes which can be occupied at those low frequencies. Please mind, the graph shows a very steep gradient close to 0 cm^{-1} because of the quickly growing phonon lifetime for low frequencies, however, contribution to thermal conductivity is not diverging because of vanishing group velocities at the Γ point.

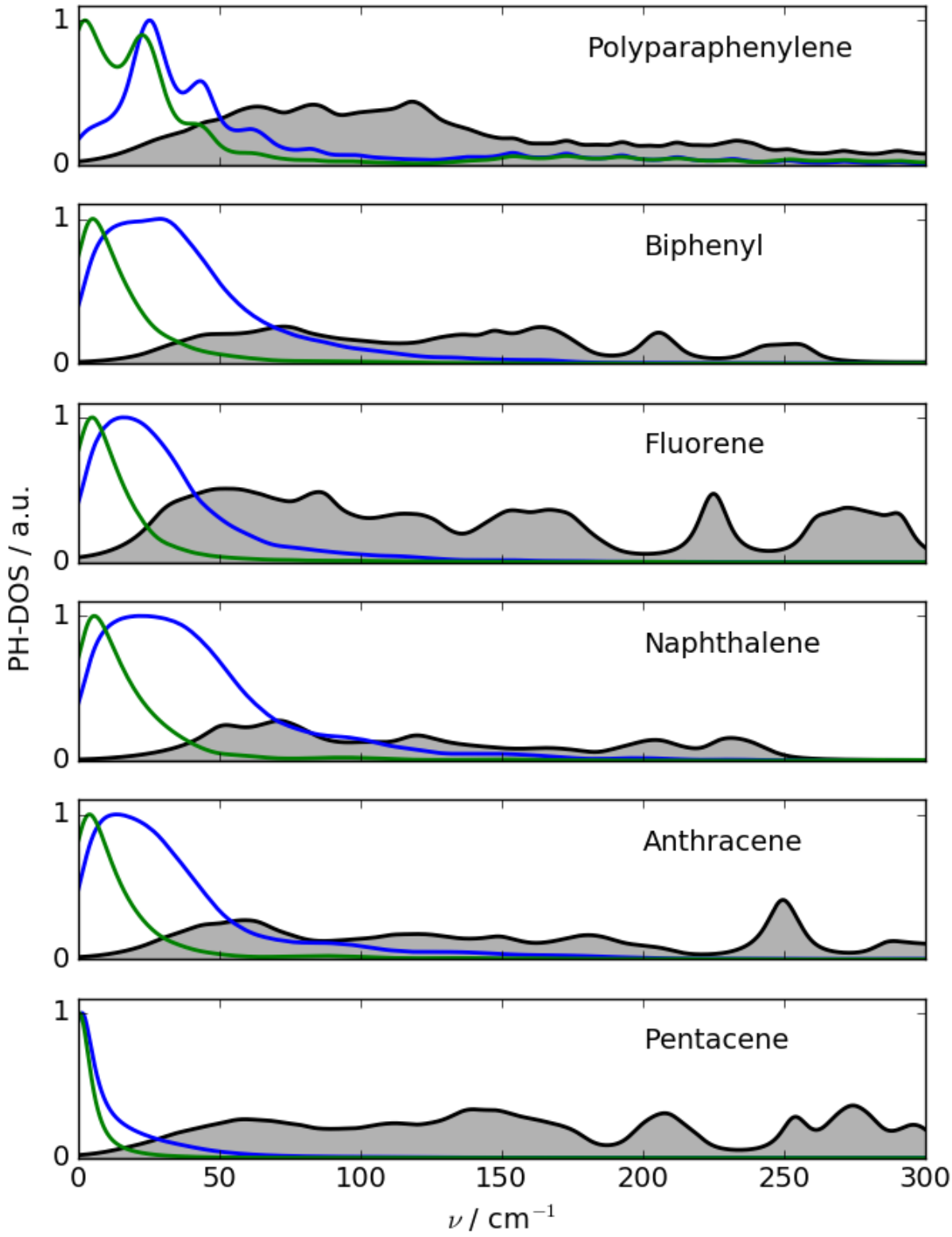

Figure 26: Mode dependent phonon contribution to thermal conductivity (green) and its product with the phonon density of states (blue). The phonon density of states is plotted in black and filled. σ = 5 cm^{-1}.

Within the used approach two contributions, the heat capacity and phonon lifetime are temperature dependent, however they affect kappa at different temperature regimes. The phonon model accounts for phonon-phonon scattering which is dominant at elevated temperatures. For 10K the FWHM of the heat capacity function is still 25cm^{-1}, which is still the same frequency range for sufficiently large phonon lifetimes. The effects caused by heat capacity are therefore only relevant at even lower temperatures below 10K. For the tested materials thermal conductivities show temperature dependence up to around 200K and stay constant for higher temperatures. Figure 27 illustrates the temperature dependence of the yy-component of the thermal conductivity tensor for the materials fluorene and polyparaphenylene. This trend is exhibited by the other investigated materials too and also valid for the other components of the thermal conductivity tensor but are omitted in Figure 27 to allow for a clear presentation.

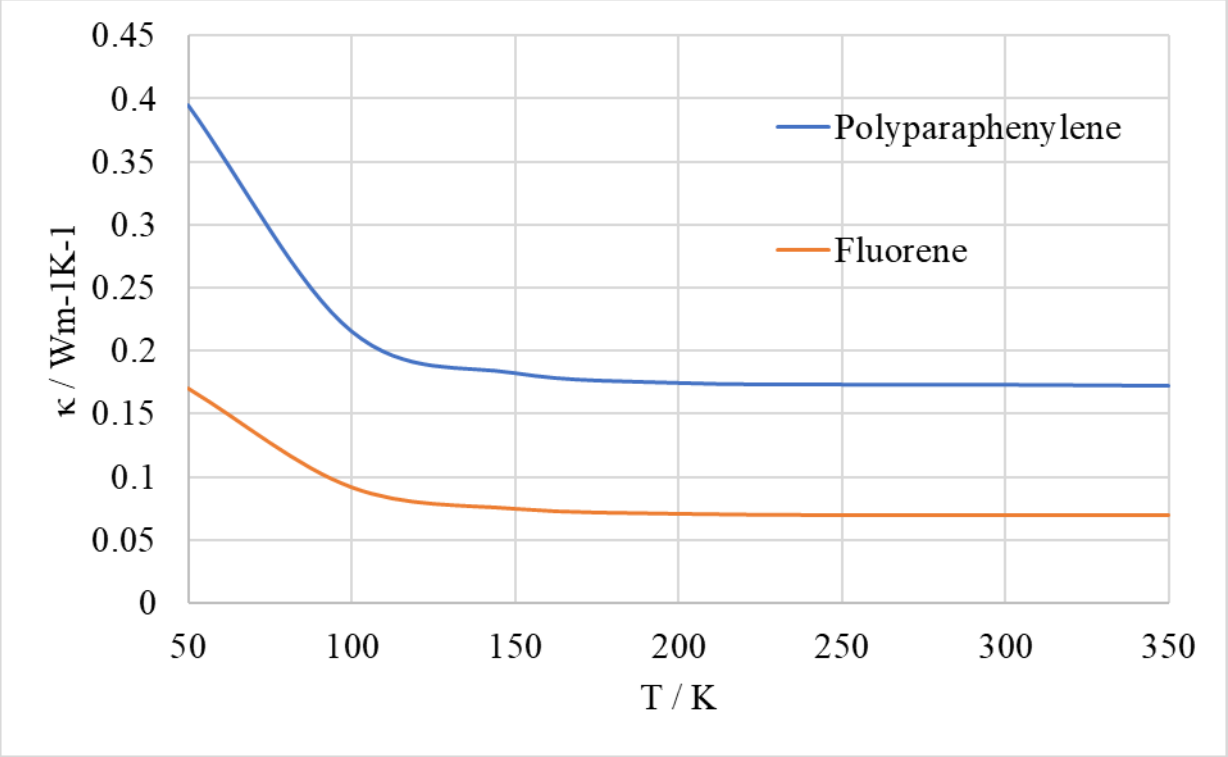

Figure 27: Temperature dependence of calculated thermal conductivites shown examplary for fluorene and polyparaphenylene.

Since all the tested materials have crystal structures which are non-cubic, thermal conductivity as a property must obey Neumann's principle. It states, that properties of a crystal must show the point group symmetry of the crystal structure. On top of that, the molecules forming organic crystals are not of spherical shape like atoms, but rather they are three dimensional objects adding an additional

component to anisotropic behavior due to anisotropic interactions. In Figure 28 the main components of the thermal conductivity tensor (xx, yy, zz) are plotted. All investigated materials are oriented in a way, that the components xx and yy represent the thermal conductivity within the molecular layers (in-plane). The zz component illustrates the thermal conductivity perpendicular to the layered structure (out-of-plane).

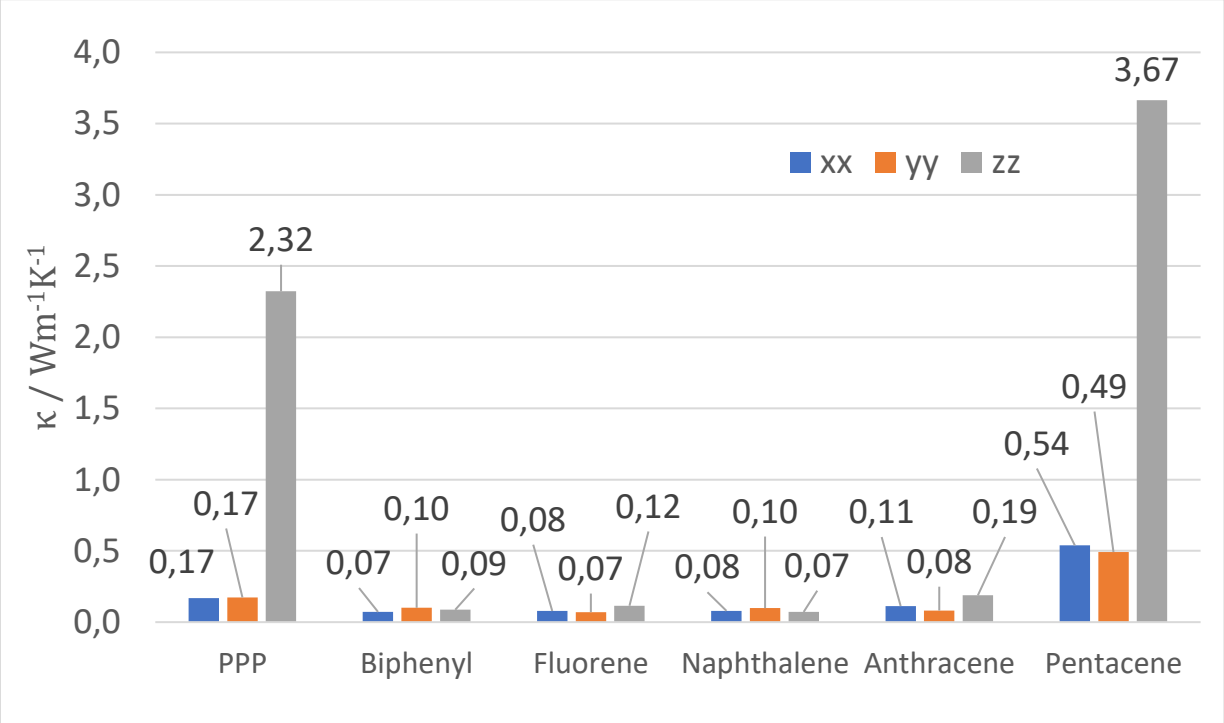

Figure 28: Main components (xx, yy, zz) of the thermal conductivity tensor at 300K.

For all materials the in-plane thermal conductivities (xx and yy components of the thermal conductivity tensor) are very similar and show negligible directional dependence. Furthermore, concerning the small molecules biphenyl, fluorene and naphthalene the out-of-plane and in-plane thermal conductivities are very similar too and do not show any directional dependence for the thermal conductivity. The other materials polyparaphenylene, anthracene and pentacene show a pronounced anisotropy with a drastically increased out-of-plane thermal conductivity. This behavior will be part of the following discussion.

To assess the reliability of the employed approach, the obtained thermal conductivities should be compared to experimental data. Unfortunately, there is only few experimental data available. To the best of my knowledge, there are experimental values of the thermal conductivity only for biphenyl and naphthalene. The values for biphenyl range from 0.37 W/mK at 303 K to 0.29 W/mK

at 334 K[79]. Compared to the obtained value at 300 K the experimental value is around 4 times larger than the calculated one. For naphthalene the experimental value of 2.31 W/mK obtained by B. M. Mogilevskii and V. G. Surin (as cited in Slack, 1979)[80] differs a lot compared to the calculated result, however, it should be noted that the thermal conductivity was measured just below the melting point (353 K)[81]. The agreement between calculated and experimental values is rather poor, which could probably be resolved by refitting of the phonon lifetime model. However, due to the lack of experimentally obtained thermal conductivities more elaborate methodologies to account for the phonon lifetimes would be required, to fit the phonon lifetime model.

5. Discussion

As a quick reminder, the main goals of this thesis were to model thermal transport in molecular crystals and subsequently, to establish structure-to-property relationships concerning thermal transport for this class of materials. So far, the theory and applied workflow to calculate the thermal conductivity have been discussed and the thermal conductivities and all the ingredients to it have been shown. Therefore, the focus of this chapter lies on discussing the calculated results to derive structure-to-property relationships. Figure 1 illustrates the investigated materials which were chosen to study the effects of the torsional degree of freedom (DOF) and varying molecular size. Already mentioned above, it should be noted that the anisotropy of the thermal conductivity in this work solely stems from the group velocities (see section 2.4). In the following, first the effects of different molecular size on thermal transport are discussed and subsequently, the influence of the torsional DOF on thermal conductivity is examined.

5.1. Structure-to-property relationships: Size effects

In Figure 28 the components of the thermal conductivity tensor are illustrated. This plot shows, that the ratio between out-of-plane and in-plane thermal conductivity changes dramatically with increasing size. This trend is present for the materials biphenyl and polyparaphenylene as well as for the three investigated acenes.

For the smallest acene, naphthalene, all three components of the thermal conductivity tensor are very similar and don’t show a preferred direction for thermal transport. The slightly larger anthracene, containing three fused benzene rings, exhibits an out-of-plane thermal conductivity which is roughly double the in-plane conductivity. In the case of pentacene, the thermal conductivity normal to the layers of the crystal structure is more than 7 times larger than within the

layers. As the anisotropy of the thermal conductivity calculated according to the proposed methodology solely stems from the directional dependence of the group velocities, the present trend leads to the assumption, that for larger molecules the group velocities are higher and more confined along the molecule's orientation. Furthermore, the MSGP characterizing the internal anharmonicity steadily decreases from naphthalene over anthracene to pentacene (see Table 4). With increasing size of the molecules, also the thickness of densely packed layers increases, which in return means, that for a given length, less molecular layers and also less interfaces between the layers are present. This leads to the conclusion, that a reduced number of interfaces between the layers reduces the internal anharmonicity. This relates then to increased phonon lifetimes and therefore the thermal conductivity is increased.

Both aspects are also valid for the phenylenes, biphenyl and polyparaphenylene. Due to the stronger interactions of the covalent bonds along the polymer chain, the group velocities in polyparaphenylene are drastically higher than in biphenyl. In contrast to the acenes where the number of interfaces decreased with increasing molecular size, polyparaphenylene is modeled in this work as an infinite chain without any layers and therefore also no interfaces between them. Again, the MSGP of polyparaphenylene is a lot lower than for biphenyl, which leads to increased phonon lifetimes and thermal conductivity.

5.2. Structure-to-property relationships: Effects of the torsional degree of freedom

The second part of structure-to-property related research question is concerned about the torsional stiffness of the molecule and how this affects thermal conductivity. Judging the influence of this structural property on the thermal conductivity by comparing the results for naphthalene, fluorene and biphenyl, no clear trend is obvious. For further discussion, the eigenmodes and their symmetry at the Γ point were investigated. In Figure 27, the phonon DOS (mesh-sampling on 15x15x15 grid, broadening σ = 1 cm^{-1}) is plotted over a frequency range up to 500 cm^{-1} and the frequencies at the Γ point of eigenmodes with either out-of-plane bending, twisting or in-plane bending symmetry are highlighted. As expected, according to the equation for undamped oscillation of a simple spring, $\omega = \sqrt{k/m}$ with the spring constant k and the mass m, the structural differences in torsional and bending stiffness are visible in the phonon DOS. The additional methylene group in fluorene should increase the moment of resistance, thus increasing the frequencies of the considered modes. However, due to the increased mass of fluorene compared to biphenyl, the frequency shift is rather

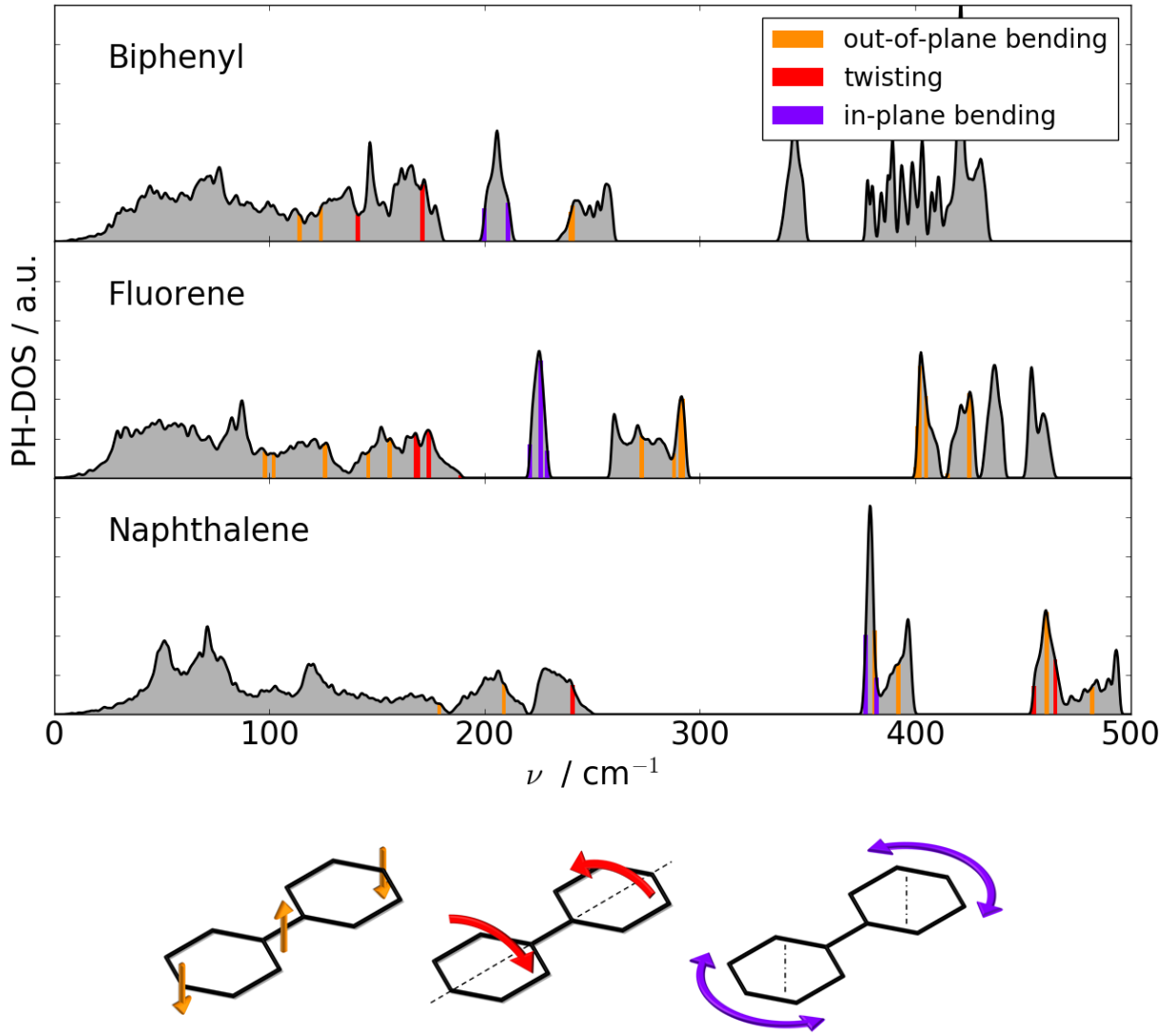

Figure 29: Phonon DOS with modes of special symmetry highlighted at the Γ point.

small. Naphthalene on the other hand is even more lightweight than biphenyl and considering the increased moment of resistance against bending and torsion, the considered modes show a large shift in frequency. Especially the in-plane bending modes (violet lines) are of much higher frequency for naphthalene (377, 382 cm^{-1}) compared to biphenyl (200, 211 cm^{-1}) and fluorene (221, 226, 229 cm^{-1}). The twisting modes (red lines) are of certainly higher frequency too (241, 455, 465 cm^{-1}) compared to biphenyl's (141, 171 cm^{-1}) and fluorene's (168, 169, 174, 189 cm^{-1}).

Within the chosen modelling approach, the lifetimes for those frequencies are vanishing, thus they deny any contribution to the thermal conductivity. For further inspection of this issue, a more elaborate method to account for phonon lifetimes is required. A valid approach would be

anharmonic lattice dynamics, which allows to calculate phonon lifetimes per mode. Considering this lifetime model, changes in torsional degree of freedom don’t affect the thermal conductivity.

References

1. Zhao, L.-D. *et al.* Ultralow thermal conductivity and high thermoelectric figure of merit in SnSe crystals. *Nature* **508,** 373–377 (2014).

2. Tritt, T. M. *Thermal Conductivity: Theory, properties and apllications*. *Journal of Chemical Information and Modeling* **53,** (2004).

3. Klauk, H. Organic Electronics Materials, Manufacturing and Applications. *Wiley-VCH* (2006).

4. Kim, N. *et al.* Thermal transport properties of thin films of small molecule organic semiconductors. *Appl. Phys. Lett.* **87,** 241908 (2005).

5. Bubnova, O. & Crispin, X. Towards polymer-based organic thermoelectric generators. *Energy Environ. Sci.* **5,** 9345–9362 (2012).

6. Torizuka, K., Tajima, H., Kawamura, Y., Sawa, H. & Yamamoto, T. Thermal transport of organic molecular crystals (DMe-DCNQI)2Li(1−x)Cux and observation of their super-lattice structure by means of synchrotron radiation X-ray. *J. Phys. Chem. Solids* **66,** 1575–1578 (2005).

7. Duda, J. C., Hopkins, P. E., Shen, Y. & Gupta, M. C. Thermal transport in organic semiconducting polymers. *Appl. Phys. Lett.* **102,** 251912 (2013).

8. Kaul, P. B., Day, K. A. & Abramson, A. R. Application of the three omega method for the thermal conductivity measurement of polyaniline. *J. Appl. Phys.* **101,** 083507 (2007).

9. Wang, X., Liman, C. D., Treat, N. D., Chabinyc, M. L. & Cahill, D. G. Ultralow thermal conductivity of fullerene derivatives. *Phys. Rev. B* **88,** 075310 (2013).

10. Shen, S., Henry, A., Tong, J., Zheng, R. & Chen, G. Polyethylene nanofibres with very high thermal conductivities. *Nat. Nanotechnol.* | **5,** (2010).

11. Shrestha, R. *et al.* Crystalline polymer nanofibers with ultra-high strength and thermal conductivity. *Nat. Commun.* **9,** 1664 (2018).

12. Schwoerer, M. & Wolf, H. C. *Organic Molecular Solids*. *Organic Molecular Solids* (2008).

doi:10.1002/9783527618651

13. Venkataraman, G. & Sahni, V. C. External vibrations in complex crystals. *Rev. Mod. Phys.* **42,** 409–470 (1970).

14. Bergwerf, H. MolView: an attempt to get the cloud into chemistry classrooms. in (ed. Robert E. Belford, R. S.) (CCCE, 2015).

15. Stackhouse, S. & Stixrude, L. Theoretical Methods for Calculating the Lattice Thermal Conductivity of Minerals. *Rev. Mineral. Geochemistry* **71,** 253–269 (2010).

16. Green, M. S. Markoff Random Processes and the Statistical Mechanics of Time-Dependent Phenomena. II. Irreversible Processes in Fluids. *J. Chem. Phys.* **22,** 398–413 (1954).

17. Kubo, R. Statistical-Mechanical Theory of Irreversible Processes. I. General Theory and Simple Applications to Magnetic and Conduction Problems. *J. Phys. Soc. Japan* **12,** 570–586 (1957).

18. Kubo, R. The fluctuation-dissipation theorem. *Reports Prog. Phys.* **29,** 306 (1966).

19. Müller-Plathe, F. A simple nonequilibrium molecular dynamics method for calculating the thermal conductivity. *J. Chem. Phys.* **106,** 6082–6085 (1997).

20. Jund, P. & Jullien, R. Molecular-dynamics calculation of the thermal conductivity of vitreous silica. *Phys. Rev. B* **59,** 13707–13711 (1999).

21. Schelling, P. K., Phillpot, S. R. & Keblinski, P. Comparison of atomic-level simulation methods for computing thermal conductivity. *Phys. Rev. B* **65,** 144306 (2002).

22. Alfè, D. PHON: A program to calculate phonons using the small displacement method. *Comput. Phys. Commun.* **180,** 2622–2633 (2009).

23. Baroni, S., De Gironcoli, S., Dal Corso, A. & Giannozzi, P. Phonons and related crystal properties from density-functional perturbation theory. *Rev. Mod. Phys.* **73,** 515–562 (2001).

24. Turney, J. E., Landry, E. S., McGaughey, A. J. H. & Amon, C. H. Predicting phonon properties and thermal conductivity from anharmonic lattice dynamics calculations and molecular dynamics simulations. *Phys. Rev. B* **79,** 064301

25. de Koker, N. Thermal Conductivity of MgO Periclase from Equilibrium First Principles

Molecular Dynamics. *Phys. Rev. Lett.* **103,** 125902 (2009).

26. Birner, G., Mingo, N., Stewart, D. A., Malorny, M. & Broido, D. A. Intrinsic lattice thermal conductivity of semiconductors from first principles. *Appl. Phys. Lett.* **91,** 231922 (2007).

27. Callaway, J. Model for Lattice Thermal Conductivity at Low Temperatures. *Phys. Rev.* **113,** 1046–1051 (1959).

28. Slack, G. A. & Galginaitis, S. Thermal conductivity and phonon scattering by magnetic impurities in CdTe. *Phys. Rev.* **133,** (1964).

29. Gross, R. & Marx, A. *Festkörperphysik*. (De Gruyter, 2014).

30. Ashcroft, N. W. & Mermin, N. D. *Solid state physics*. (Saunders College Publishing, 1976).

31. Bjerg, L., Iversen, B. B. & Madsen, G. K. H. Modeling the thermal conductivities of the zinc antimonides ZnSb and Zn 4 Sb 3. *Phys. Rev. B - Condens. Matter Mater. Phys.* **89,** 1–8 (2014).

32. Slack, G. A. The Thermal Condcutivity of Nonmetallic Crystals. *Solid State Phys.* **34,** (1979).

33. Leibfried, G. & Schlömann, E. ,. *Nachr. Adkad. Wiss. Göttingen, Math-Phys., Klasse 4, 71* (1954).

34. Tkatchenko, A. & Scheffler, M. Accurate Molecular Van Der Waals Interactions from Ground-State Electron Density and Free-Atom Reference Data. *Phys. Rev. Lett.* **102,** 073005 (2009).

35. Grimme, S., Antony, J., Ehrlich, S. & Krieg, H. A consistent and accurate ab initio parametrization of density functional dispersion correction (DFT-D) for the 94 elements H-Pu. *J. Chem. Phys.* **132,** 154104 (2010).

36. Sholl, D. S. & Steckel, J. A. *Density Functional Theory*. (John Wiley & Sons, Inc., 2009). doi:10.1002/9780470447710

37. Hohenberg, P. & Kohn, W. Inhomogeneous Electron Gas. *Phys. Rev.* **136,** B864–B871 (1964).

38. Fiolhais, C., Nogueira, F. & Marques, M. A. L. *A Primer in Density Functional Theory*.

(Springer Berlin Heidelberg, 2003). doi:10.1007/3-540-37072-2

39. Kohn, W. & Sham, L. J. Self-Consistent Equations Including Exchange and Correlation Effects. *Phys. Rev.* **140,** A1133–A1138 (1965).

40. Perdew, J. P., Burke, K. & Ernzerhof, M. *Generalized Gradient Approximation Made Simple*. *Physical Review Letters* **77,** 3865–3868 (American Physical Society, 1996).

41. Krüger, T., Elstner, M., Schiffels, P. & Frauenheim, T. Validation of the density-functional based tight-binding approximation method for the calculation of reaction energies and other data. *J. Chem. Phys.* **122,** 114110 (2005).

42. Nikolaj Otte, Mirjam Scholten, and & Thiel*, W. Looking at Self-Consistent-Charge Density Functional Tight Binding from a Semiempirical Perspective†. (2007). doi:10.1021/JP0700130

43. Aradi, B., Hourahine, ‡ B & Frauenheim, T. DFTB+, a Sparse Matrix-Based Implementation of the DFTB Method †. (2007). doi:10.1021/jp070186p

44. Porezag, D., Frauenheim, T., Köhler, T., Seifert, G. & Kaschner, R. Construction of tight-binding-like potentials on the basis of density-functional theory: Application to carbon. *Phys. Rev. B* **51,** 12947–12957 (1995).

45. Elstner, M. *et al. Self-consistent-charge density-functional tight-binding method for simulations of complex materials properties*. (1998).

46. Yang, Y. *et al.* Extension of the Self-Consistent-Charge Density-Functional Tight-Binding Method: Third-Order Expansion of the Density Functional Theory Total Energy and Introduction of a Modified Effective Coulomb Interaction. (2007). doi:10.1021/jp074167r

47. Elstner, M. & Seifert, G. Density functional tight binding. *Philos. Trans. R. Soc. A Math. Phys. Eng. Sci.* **372,** 20120483–20120483 (2014).

48. Marcus A. Neumann*, † and & Perrin‡, M.-A. Energy Ranking of Molecular Crystals Using Density Functional Theory Calculations and an Empirical van der Waals Correction. (2005). doi:10.1021/JP050121R

49. von Lilienfeld, O. A., Tavernelli, I., Rothlisberger, U. & Sebastiani, D. Optimization of Effective Atom Centered Potentials for London Dispersion Forces in Density Functional

Theory. *Phys. Rev. Lett.* **93,** 153004 (2004).

50. Chai, J.-D. & Head-Gordon, M. Long-range corrected hybrid density functionals with damped atom–atom dispersion corrections. *Phys. Chem. Chem. Phys.* **10,** 6615 (2008).

51. Bedoya-Martínez, N. *et al.* Toward a Reliable Description of the Lattice Vibrations in Organic Molecular Crystals: The Impact of van der Waals Interactions. (2018). doi:10.1021/acs.jctc.8b00484

52. Groom, C. R., Bruno, I. J., Lightfoot, M. P., Ward, S. C. & IUCr. The Cambridge Structural Database. *Acta Crystallogr. Sect. B Struct. Sci. Cryst. Eng. Mater.* **72,** 171–179 (2016).

53. Trotter, J. The crystal and molecular structure of biphenyl. *Acta Crystallogr.* **14,** 1135–1140 (1961).

54. Belsky, V. K., Zavodnik, V. E. & Vozzhennikov, V. M. Fluorene, C13H10. *Acta Crystallogr. Sect. C Cryst. Struct. Commun.* **40,** 1210–1211 (1984).

55. Capelli, S. C., Albinati, A., Mason, S. A. & Willis, B. T. M. Molecular motion in crystalline naphthalene: Analysis of multi-temperature X-ray and neutron diffraction data. *J. Phys. Chem. A* **110,** 11695–11703 (2006).

56. Brock, C. P. & Dtrnitz, J. D. *Temperature Dependence of Thermal Motion in Crystalline Anthracene*. *Acta Cryst* **46,** (1990).

57. Mattheus, C. C. *et al.* Polymorphism in pentacene. *Acta Crystallogr. Sect. C Cryst. Struct. Commun.* **57,** 939–941 (2001).

58. Ambrosch-Draxl, C., Majewski, J. A., Vogl, P. & Leising, G. First-principles studies of the structural and optical properties of crystalline poly(para-phenylene). *Phys. Rev. B* **51,** 9668–9676 (1995).

59. Gaus, M., Goez, A. & Elstner, M. Parametrization and benchmark of DFTB3 for organic molecules. *J. Chem. Theory Comput.* **9,** 338–354 (2013).

60. Kresse, G. & Hafner, J. Ab initio molecular dynamcis for liquid metals. *Phys. Rev. B* **47,** 558 (1993).

61. Kresse, G. & Hafner, J. Ab initio molecular-dynamics simulation of the liquid-metal–

amorphous-semiconductor transition in germanium. *Phys. Rev. B* **49,** 14251–14269 (1994).

62. Kresse, G. & Furthmüller, J. Efficiency of ab-initio total energy calculations for metals and semiconductors using a plane-wave basis set. *Comput. Mater. Sci.* **6,** 15–50 (1996).

63. Kresse, G. & Furthmüller, J. Efficient iterative schemes for ab initio total-energy calculations using a plane-wave basis set. *Phys. Rev. B* **54,** 11169–11186 (1996).

64. Kresse, G. & Joubert, D. From ultrasoft pseudopotentials to the projector augmented-wave method. *Phys. Rev. B* **59,** 1758–1775 (1999).

65. Monkhorst, H. J. & Pack, J. D. Special points for Brillouin-zone integrations. *Phys. Rev. B* **13,** 5188–5192 (1976).

66. Bučko, T., Hafner, J. & Ángyán, J. G. Geometry optimization of periodic systems using internal coordinates. *J. Chem. Phys.* **122,** 124508 (2005).

67. Lindh, R., Bernhardsson, A., Karlström, G. & Malmqvist, P. Å. On the use of a Hessian model function in molecular geometry optimizations. *Chem. Phys. Lett.* **241,** 423–428 (1995).

68. BROYDEN, C. G. The Convergence of a Class of Double-rank Minimization Algorithms 1. General Considerations. *IMA J. Appl. Math.* **6,** 76–90 (1970).

69. Fletcher, R. A new approach to variable metric algorithms. *Comput. J.* **13,** 317–322 (1970).

70. Goldfarb, D. A family of variable-metric methods derived by variational means. *Math. Comput.* **24,** 23–23 (1970).

71. Shanno, D. F. Conditioning of quasi-Newton methods for function minimization. *Math. Comput.* **24,** 647–647 (1970).

72. Stöhr, M., Michelitsch, G. S., Tully, J. C., Reuter, K. & Maurer, R. J. Communication: Charge-population based dispersion interactions for molecules and materials. *J. Chem. Phys.* **144,** (2016).

73. Gaus, M., Cui, Q. & Elstner, M. DFTB3: Extension of the self-consistent-charge density-functional tight-binding method (SCC-DFTB). *J. Chem. Theory Comput.* **7,** 931–948 (2011).

74. Togo, A. & Tanaka, I. First principles phonon calculations in materials science. *Scr. Mater.* **108,** 1–5 (2015).

75. Baudour, J. L., Cailleau, H., Yelon, W. B. & IUCr. Structural phase transition in polyphenyls. IV. Double-well potential in the disordered phase of *p* -terphenyl from neutron (200 K) and X-ray (room-temperature) diffraction data. *Acta Crystallogr. Sect. B Struct. Crystallogr. Cryst. Chem.* **33,** 1773–1780 (1977).

76. Baudour, J. L. & IUCr. Structural phase transition in polyphenyls. X. Potential barrier heights in crystalline polyphenyls and in gaseous biphenyl determined uniquely from diffraction data. *Acta Crystallogr. Sect. B Struct. Sci.* **47,** 935–949 (1991).

77. Setyawan, W. & Curtarolo, S. High-throughput electronic band structure calculations: Challenges and tools. *Comput. Mater. Sci.* **49,** 299–312 (2010).

78. Li, W., Carrete, J., Madsen, G. K. H. & Mingo, N. Influence of the optical-acoustic phonon hybridization on phonon scattering and thermal conductivity. *Phys. Rev. B* **93,** (2016).

79. Ohki, K. & Kowalczyk, L. S. Thermal Conductivity of Some Organic Compounds at Their Melting Points. *J. Chem. Eng. Data* **9,** 220–221 (1964).

80. Slack, G. A. The Thermal Conductivity of Nonmetallic Crystals. *Solid State Phys. - Adv. Res. Appl.* **34,** 1–71 (1979).

81. O'Neil, M. J. *The Merck Index - An Encyclopedia of Chemicals, Drugs, and Biologicals*. (UK: Royal Society of Chemistry, 2013).

82. Momma, K. & Izumi, F. VESTA 3 for three-dimensional visualization of crystal, volumetric and morphology data. *J. Appl. Crystallogr.* **44,** 1272–1276 (2011).

List of Figures

APPENDIX A – Band structures: VASP+TS vs. DFTB3+D3-BJ

Fluorene

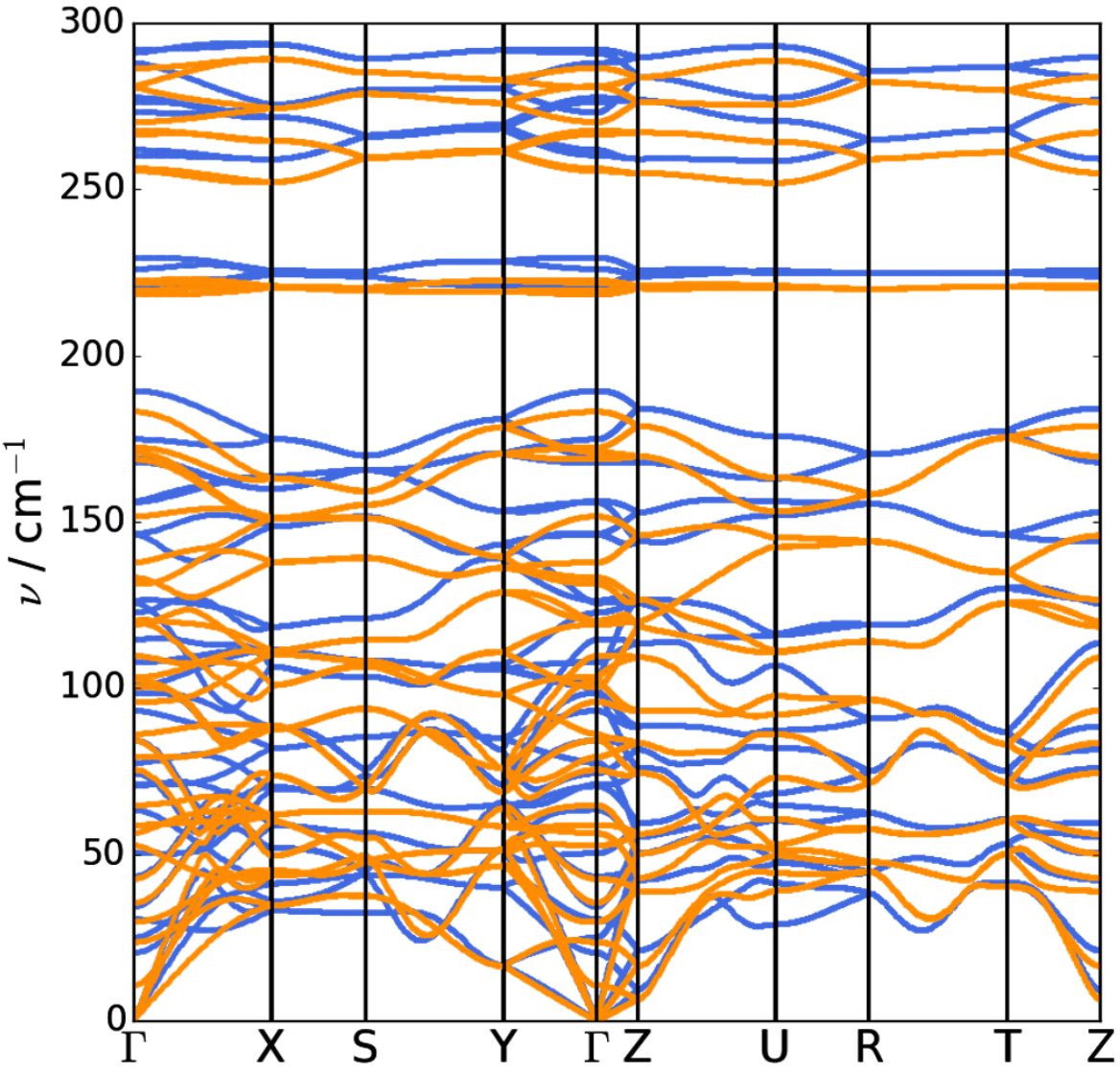

Figure 30: Comparison of the band structure of fluorene obtained with VASP+TS (orange) and DFTB+D3-BJ (blue)

Naphthalene

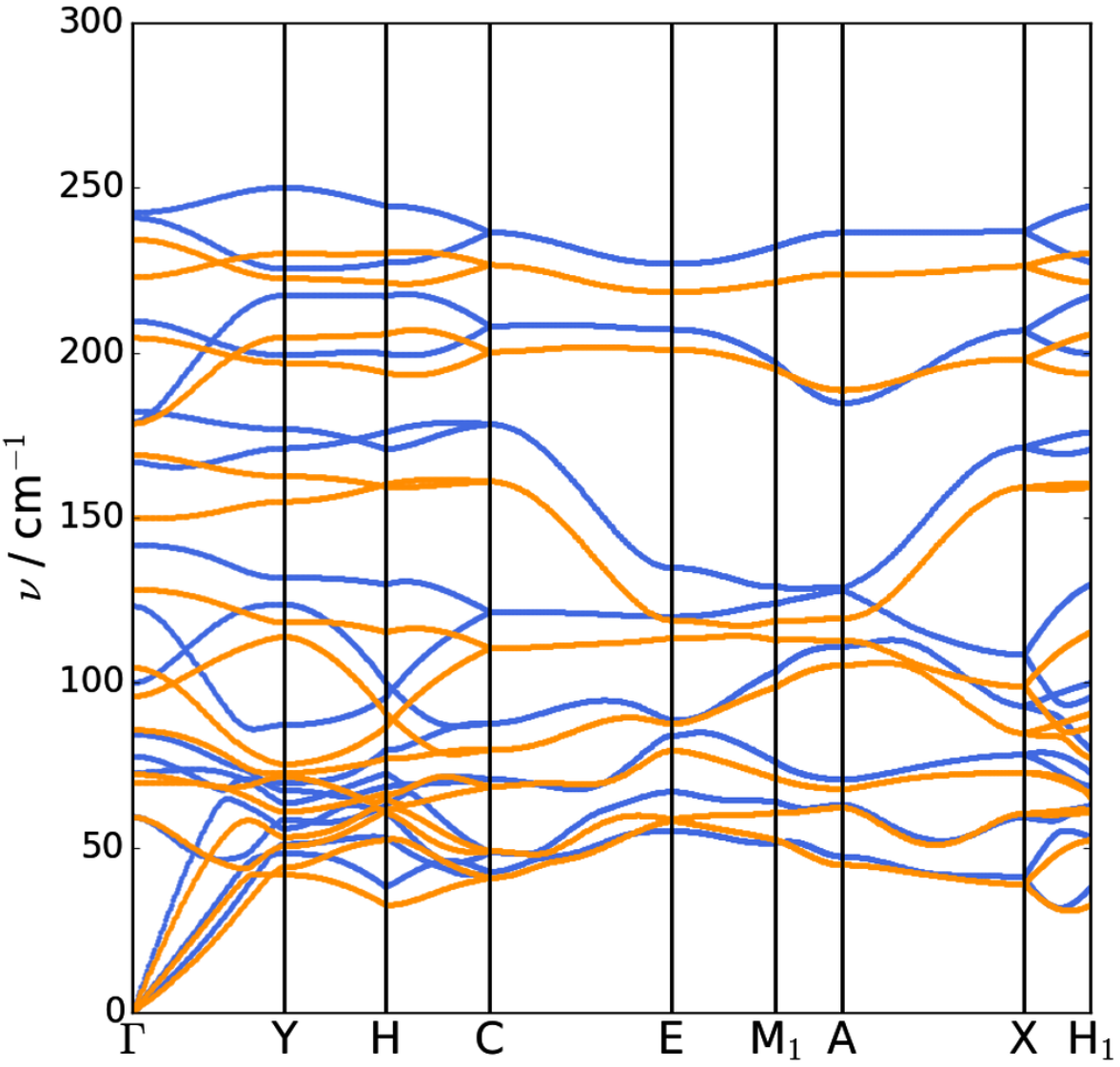

Figure 31: Comparison of the band structure of naphthalene obtained with VASP+TS (orange) and DFTB+D3-BJ (blue)